Summer 2008

Petrogenetic Processes Characterizing the Mount Bachelor, Oregon Magmatic System: Open- versus Closed-System Processes

Sara Elizabeth Johnson
Central Washington University

PETROGENETIC PROCESSES CHARACTERIZING THE MOUNT BACHELOR, OREGON MAGMATIC SYSTEM: OPEN- VERSUS CLOSED-SYSTEM PROCESSES

A Thesis

Presented to

The Graduate Faculty

Central Washington University

In Partial Fulfillment

of the Requirements for the Degree

Master of Science

Geology

---

by

Sara Elizabeth Johnson

August 2008

CENTRAL WASHINGTON UNIVERSITY

Graduate Studies

We hereby approve the thesis of

Sara Elizabeth Johnson

Candidate for the degree of Master of Science

APPROVED FOR THE GRADUATE FACULTY

_____	_____
	Dr. Wendy Bohrson, Committee Chair
_____	_____
	Dr. Carey Gazis
_____	_____
	Dr. Rick Conrey
_____	_____
	Cynthia Gardner
_____	_____
	Dean of Graduate Studies

ABSTRACT

PETROGENETIC PROCESSES CHARACTERIZING THE
MOUNT BACHELOR, OREGON MAGMATIC SYSTEM:
OPEN- VERSUS CLOSED-SYSTEM PROCESSES

by

Sara Elizabeth Johnson

August 2008

Mount Bachelor volcanic chain (MBVC), located in central Oregon, is one of the larger basalt and basaltic-andesite edifices in central Oregon. Preliminary studies have defined how eruptions have changed composition with time, but a detailed assessment of magma chamber processes has not been conducted. To gain a more thorough understanding of the magmatic processes that have contributed to the observed compositional evolution, this study focuses on one of four eruptive episodes, specifically episode III, the most voluminous episode of the four. Magmatic processes are assessed by focusing on both whole-rock and single crystal data.

The geochemistry and textural diversity of twenty representative lavas were determined to elucidate the associated magmatic processes. Magmatic systems can be impacted by external influences, such as the incorporation of melt from the rock surrounding a magma chamber (assimilation), or the replenishment of magma from below (recharge). These processes result in open-system magma chambers and modify

the original chemistry of magma. Closed-system processes such as crystal formation and separation can also significantly alter the magma chemistry.

The focus of this study was to determine which of these processes was most significant in the formation of the lavas erupted during episode III, utilizing both whole-rock and single crystal geochemical and isotopic analyses. Results suggest that crystal separation in a closed magmatic system generated the majority of the geochemical diversity observed. Radiogenic isotopic disequilibrium suggests, however, that heat released during crystallization resulted in melting of surrounding country rock, and thus the incorporation of that melt into the magma system. Evidence for magma recharge events is also observed in the isotopic analyses. Geochemical distinctions between units of episode III indicate the potential for several independent magmatic reservoirs to exist beneath the MBVC. Further work, specifically the incorporation of computer modeling, will allow documentation of the physical properties of the magma system and elucidate quantitative magma chamber models. This and additional work at the MBVC may lead to a better understanding of the magma systems located under the MBVC, as well as other volcanoes located in the central Oregon High Cascades region.

ACKNOWLDGEMENTS

I would like to first and foremost thank Dr. Wendy Bohrson for all of the time she has spent with me over the past two years, enabling me to better understand igneous petrology and volcanism, as well as showing me how to become a better scientist. Without her assistance, this project would not have reached the caliber it has. Her patience and encouragement has been the most rewarding part of my experience at Central Washington University. Also, Dr. Frank Ramos, whose tutorship and guidance have provided me a lasting impression on what it means to be a geochemist. Thank you also to all my committee members, Dr. Rick Conrey, Cynthia Gardner and Dr. Carey Gazis for all of their inputs and guidance on my research project. Their ideas have contributed greatly to my understanding of the Mount Bachelor volcanic system. I would like to thank everyone who assisted me at the GeoAnalytical lab at Washington State University, Dr. Martin Streck of Portland State University who taught me how to use NDIC imaging, and Dr. Frank Tepley, III of Oregon State University who assisted me with the electron microprobe. I would also like to thank all the faculty and staff at Central Washington University, especially Vicki Potts and Craig Scrivner for all their help during the past two years.

I would like to thank my family and friends who have continued to support me over the years. Finally, I must acknowledge the students of the geology department (and various other departments too), specifically my fellow graduate students, for all of their support during the past two years.

TABLE OF CONTENTS

TABLE OF CONTENTS (continued)

LIST OF TABLES

LIST OF FIGURES

LIST OF FIGURES (continued)

CHAPTER I

INTRODUCTION

Overview

The Cascade Range is host to many volcanic chains within the Pacific Northwest region of North America. The volcanoes of this region demonstrate varied forms of volcanism, ranging from highly evolved and explosive volcanoes to more primitive, effusive eruptions. One of the most voluminous mafic chains located within the Cascade Range is the Mount Bachelor volcanic chain (MBVC), a chain of shield volcanoes, cinder cones, and lava flows, situated w

ithin the High Cascades region of central Oregon. This volcanic chain was active between 18 and 8 ka and covered an area of approximately 250 km^2 (Scott and Gardner, 1992). Eruptions at the MBVC occurred as episodes, resulting in four main periods of activity. The longest lived, most voluminous episode is episode III. This period of activity produced 25 km^3 of material and spanned a 1,000-year period. Stratigraphic relationships, eruptive volumes, and preliminary chemistry have been assessed for the MBVC (Gardner, 1994a, 1994b), yet questions remain regarding the continued evolution of the associated magma systems. Answers to these questions may provide a better understanding of the magmatic plumbing systems located under the very active Cascade Range of the Pacific Northwest.

Previous Studies

Studies conducted by Gardner and others (Gardner, 1994a, 1994b; Scott and Gardner, 1992) produced a geologic map, which provides the stratigraphic framework, as

well as characterizes the lavas of the entire MBVC. Gardner (1994b) suggested that theMBVC is composed of several magma types, ranging from basalt to basaltic-andesite, that can be divided into three distinct geochemical types. Petrologic modeling done by Gardner (1994b) suggested that the basaltic andesites of the MBVC were derived from crystal fractionation of olivine, plagioclase, clinopyroxene and magnetite; however, there is evidence in the trace elements that indicates the potential involvement of open-system processes, most likely the mixing of two magma types resulting in the third type composed of basaltic andesite. She proposed that these two magma types underwent separate evolution, indicating that at least two source areas may have existed. The data obtained by Gardner (1994b) also suggest that assimilation-fractional crystallization (AFC) processes influenced the geochemical signature of the lavas of the MBVC.

It was suggested by Gardner (1994b) that further studies focus on isotopic and rare earth element (REE) analyses to better understand the degree of AFC processes. To accomplish part of this task, this work presents geochemical and isotopic relationships for lavas from episode III, as characterized by Gardner (1994b).

Study Objectives

The objective of this study is to use whole-rock and plagioclase feldspar chemical data from lava units spanning the entirety of episode III and determine the magmatic processes that have influenced the evolution of those lavas. Magmatic plumbing systems can be affected by any combination of internal (crystal fractionation) and external (assimilation and magmatic recharge) processes, resulting in a change within the magma system. Geochemical signatures observed by analysis of whole-rock and single crystal

components can record changes in the magma system. An assessment of these components can illustrate possible magmatic processes that may have affected a magma system.

This study focused on episode III, the next to youngest and most voluminous eruptive episode of the MBVC. The episode encompasses several lava units, which from oldest to youngest are Kwohl Butte, Bachelor Shield, Bachelor Cap, and Tot Mountain. The focus of this study was to determine the potential impact that open- and closed-magmatic system processes have had on the evolution of the erupted lavas. Twenty samples that span the episode history were examined via whole-rock data, specifically textural and geochemical diversity observed by petrographic analysis, trace element geochemical information obtained from inductively coupled plasma mass spectrometry (ICP-MS), and by whole-rock $^{87}Sr/^{86}Sr$ and $^{143}Nd/^{144}Nd$ analysis.

A subset of five samples were assessed for single component geochemistry and textural diversity. Images obtained from Nomarski differential interference contrast (NDIC) microscopy were used to document plagioclase feldspar crystal textures, as well as to map areas for analysis by electron microprobe. The electron microprobe analyzes major and trace elements for selected points in plagioclase feldspar crystals. Finally, two samples from an older and younger unit of episode III were selected, ground, and handpicked for crystals for $^{87}Sr/^{86}Sr$ analysis in order to assess isotopic disequilibrium between the whole-rock and crystals.

A better understanding of magmatic systems, specifically in areas of active volcanism such as the Cascade Range and other volcanic systems, can provide information that can be utilized for volcanic hazard awareness. Assessing magmatic

processes and the resulting volcanism can provide information regarding the potential triggers of an eruption. Although the MBVC is no longer considered a potential threat, by assessing the processes affecting a magmatic system, a better understanding of magma systems and active volcanic centers can be achieved.

CHAPTER II

BACKGROUND

Geologic Setting

The MBVC is a chain of volcanic vents located in central Oregon, approximately 20 mi south of South Sister volcano and 50 mi southwest of Bend, Oregon (Figure 1). The MBVC is located along the Cascade volcanic arc that extends from southern British Columbia to northern California (Leeman et al., 2005). Arc volcanism in this region is associated with the subduction of the Juan de Fuca and Gorda plates under the North American plate (Bacon et al., 1997; Green and Sinha, 2005). In the southern portion of this arc, from Mount Adams, Washington to Lassen Peak, California, the subduction of these plates is oblique, creating widely spaced volcanoes that range from cinder cones to shield volcanoes.

The MBVC is part of the mafic platform in the High Cascades region, an area located to the east of the western Oregon Cascade Range and to the west of the Columbia Plateau. Oregon's High Cascades are unique with respect to the rest of the Pacific Northwest's Cascade Range due to the apparent primitiveness of the lavas erupted there (Hughes and Taylor, 1986; Gardner, 1994b; Schmidt et al., 2008). Throughout most of the Cascades, there is a predominance of silicic lavas, whereas approximately 85 vol % of the lavas of the central Oregon High Cascades are more mafic, ranging from basalt to basaltic andesite (Gardner, 1994b). Evidence for a rifting event originating in central Oregon at about 7 to 8 Ma, is provided by the mafic volcanic rocks, as well as the presence of a north-south oriented graben (Conrey et al., 1997). The central Oregon High

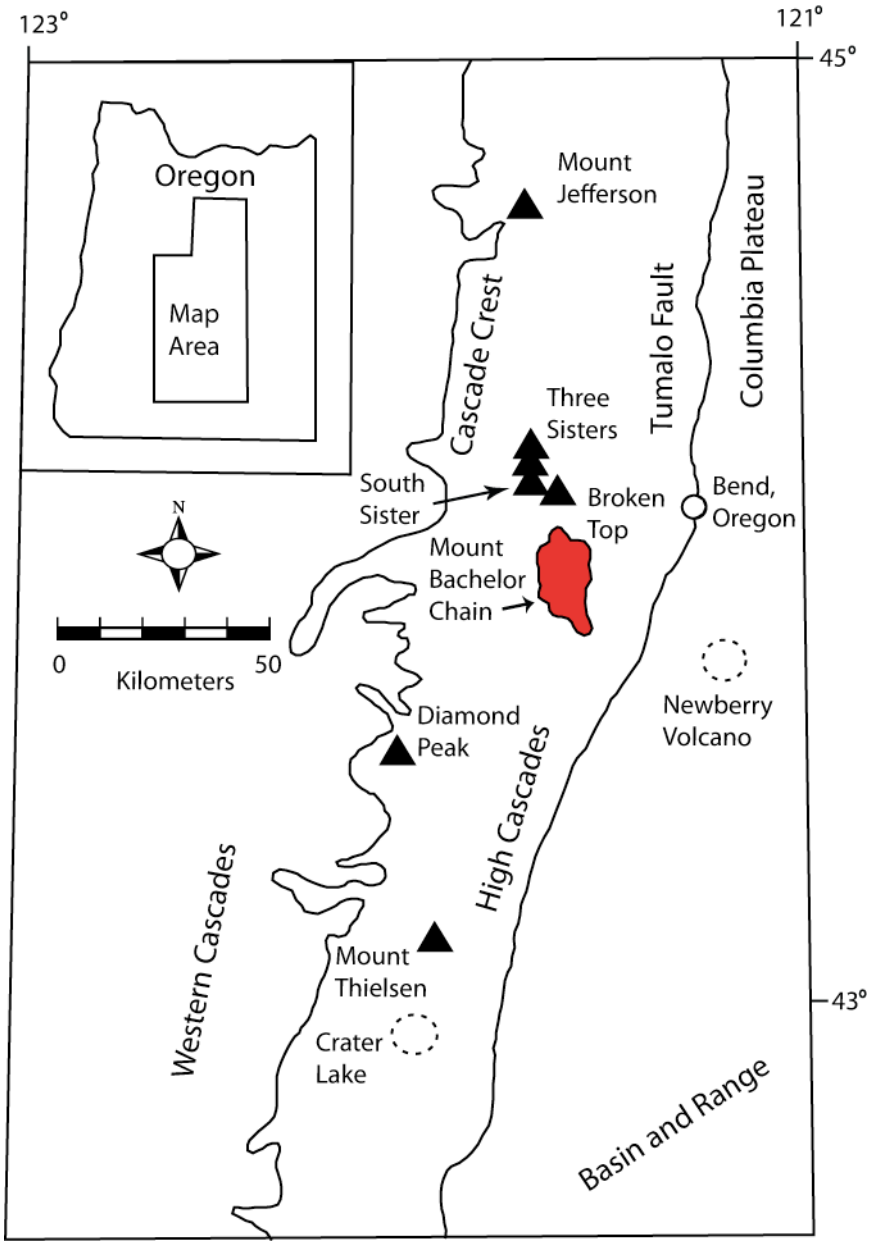

Figure 1. Geologic map of the central Oregon High Cascades. Local landmarks are included for reference (Scott and Gardner, 1990; Topinka, 1997).

Cascades are bounded by the Tumalo fault to the east and an unnamed fault along the western Cascade Range to the west (Hughes and Taylor, 1986; Conrey et al., 1997). These bounding faults, which formed by extensional tectonic processes, may provide a mechanism for eruption of the more primitive lavas observed in this region by allowing

the tapping of deeper, more primitive magma systems under the central Oregon High Cascades (Hughes and Taylor, 1986).

The MBVC is composed entirely of basalts and basaltic andesites. The chain is 25 km long; trend north-south; and consists of cinder cones, lava flows, and shield volcanoes (Scott and Gardner, 1992; Gardner, 1994b); and encompasses about 250 km^2 of central Oregon (Scott, 1990). The lavas of the MBVC erupted in four episodes, as defined by Gardner (1994b) based on paleomagnetic secular variation (PSV) studies. Lava flows were divided into the following age-related episodes (Figure 2): episode Ia includes Katsuk Butte (the oldest unit of the sequence), Red Crater, and portions of Sheridan Mountain; episode Ib includes the remainder of Sheridan Mountain and portions of Siah Butte; episode II includes the remainder of Siah Butte; episode III includes Kwohl Butte, the two components of Mount Bachelor, the Bachelor Shield and the Bachelor Cap, and Tot Mountain; and finally episode IV includes Egan Cone (Scott and Gardner, 1992; Gardner, 1994a; Gardner 1994b).

The lava flows of the MBVC are too young and/or too potassium-poor for radiometric dating techniques such as K-Ar or U-Th, and therefore, PSV analyses, along with known stratigraphic relationships, provide relative age relationships (Gardner, 1994b). Lavas were analyzed and grouped into eruptive episodes based on the similarity of paleomagnetic directions, indicating that these lavas erupted during the same time period (Gardner, 1994b). PSV analyses utilize the shift of the magnetic north pole over time and the orientation of magnetic minerals, such as Fe-Ti oxides, within the lavas. Lava flows that have similar orientations could have erupted at the same time or at a time

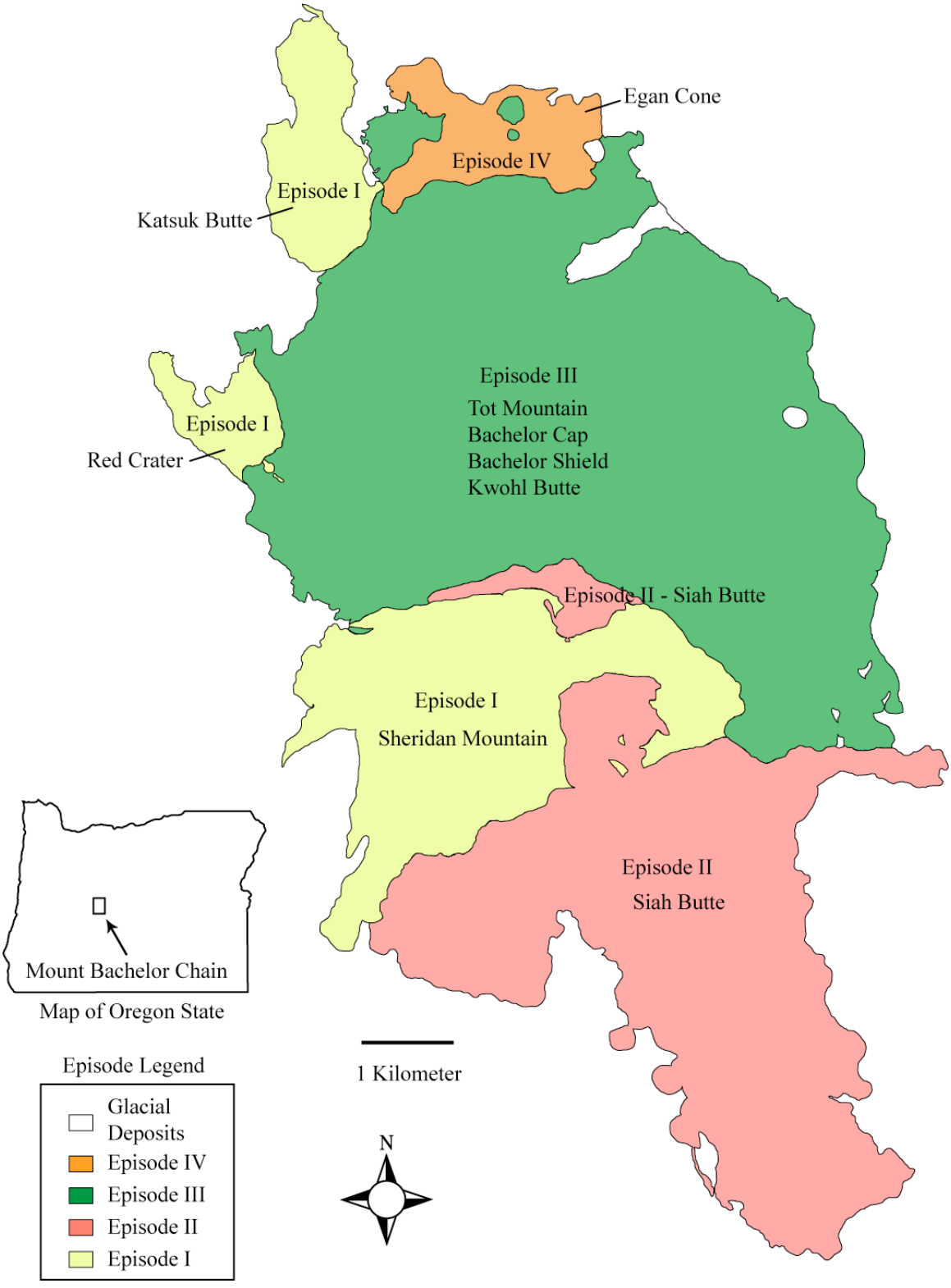

Figure 2. Geologic map of the MBVC (Gardner, 1994a).

when the secular field was oriented similarly (Champion, 1980). It is imperative that an understanding of the stratigraphic relationships is known in order for PSV analyses to be correctly interpreted.

The relative age of the oldest units at the MBVC (episode Ia and Ib) was constrained by associated glacial deposits. During the late Pleistocene, between approximately 18 and 22 ka (Scott et al., 1989; Scott, 1990), the Suttle Lake glacial advance covered the central Oregon High Cascades. The earliest erupted unit of the MBVC, Katsuk Butte, includes hyaloclastite deposits, indicating that the erupting vent(s) were located either in a lake that formed from the melting of glaciers or under ice (Scott, 1990). Katsuk Butte shows no evidence of striations or till, indicating that glaciers were not overlying the erupted material (Gardner, 1994b). Also, during the glacial retreat, end moraines were partially covered by lavas from Sheridan Mountain and Siah Butte, suggesting that volcanic activity at Mount Bachelor began during or before the glaciers were fully retreated from that region (Scott et al., 1989; Scott, 1990). Finally, scoria from the Red Crater (episode Ia) overlies unweathered till deposited by the Suttle Lake glaciers, suggesting that time between deposition of the till and scoria was short (Scott et al., 1989; Scott, 1990). These lines of evidence all indicate that the beginning of volcanic activity at the MBVC occurred simultaneously with the late Pleistocene glacial retreat from the High Cascades region of central Oregon, at approximately 18 ka.

Episode III lavas, consisting of the Bachelor–Kwohl segment, overlie flows from episodes I and II, including the Siah Butte, Sheridan Mountain, Red Crater, and Katsuk Butte segments. Within the episode III segment, the Mount Bachelor components overlie

the Kwohl Butte lavas. Tot Mountain is a vent on the south flank of Mount Bachelor Butte. Episode IV overlies the Bachelor-Kwohl segment of episode III. Egan Cone, the main component of episode IV, is overlain by Mazama ash, erupted from the Mazama Mountain eruption. The contact between these two units indicates no evidence of reworking, suggesting that the deposition of the Mazama ash occurred shortly after the cessation of eruptions at the MBVC. Bacon (1983) dated the Mazama ash at 6,850 yr B.P., constraining the youngest rocks of the MBVC to older than a minimum age of 8 ka.

This study focuses on the lavas erupted during episode III, along the Bachelor-Kwohl segment, including Kwohl Butte, Bachelor Shield and Cap, and Tot Mountain. Figure 3 depicts the four units of episode III, designated by color. According to the PSV results, the eruptive activity during the entirety of episode III were relatively brief, perhaps lasting 1,000 years or less (Gardner, 1994b). There is no evidence of a hiatus occurring during the eruptions along the Bachelor–Kwohl segment (Gardner, 1994b), although directions of lava flows from early episode III are distinctly different from those from later episode III. This indicates that the paleomagnetic directions differ during the emplacement of lavas even within the same episode, thus providing evidence that these eruptive units were emplaced between 100 and 1,000 years.

Magmatic Processes

Magmas in arc settings such as the MBVC display significant compositional diversity due to physical and chemical processes influencing the magmatic system, including partial melt generation in the mantle, crystallization, assimilation, mixing, storage, ascent, and finally, eruption (Fowler et al., 2004). Oftentimes, closed-system

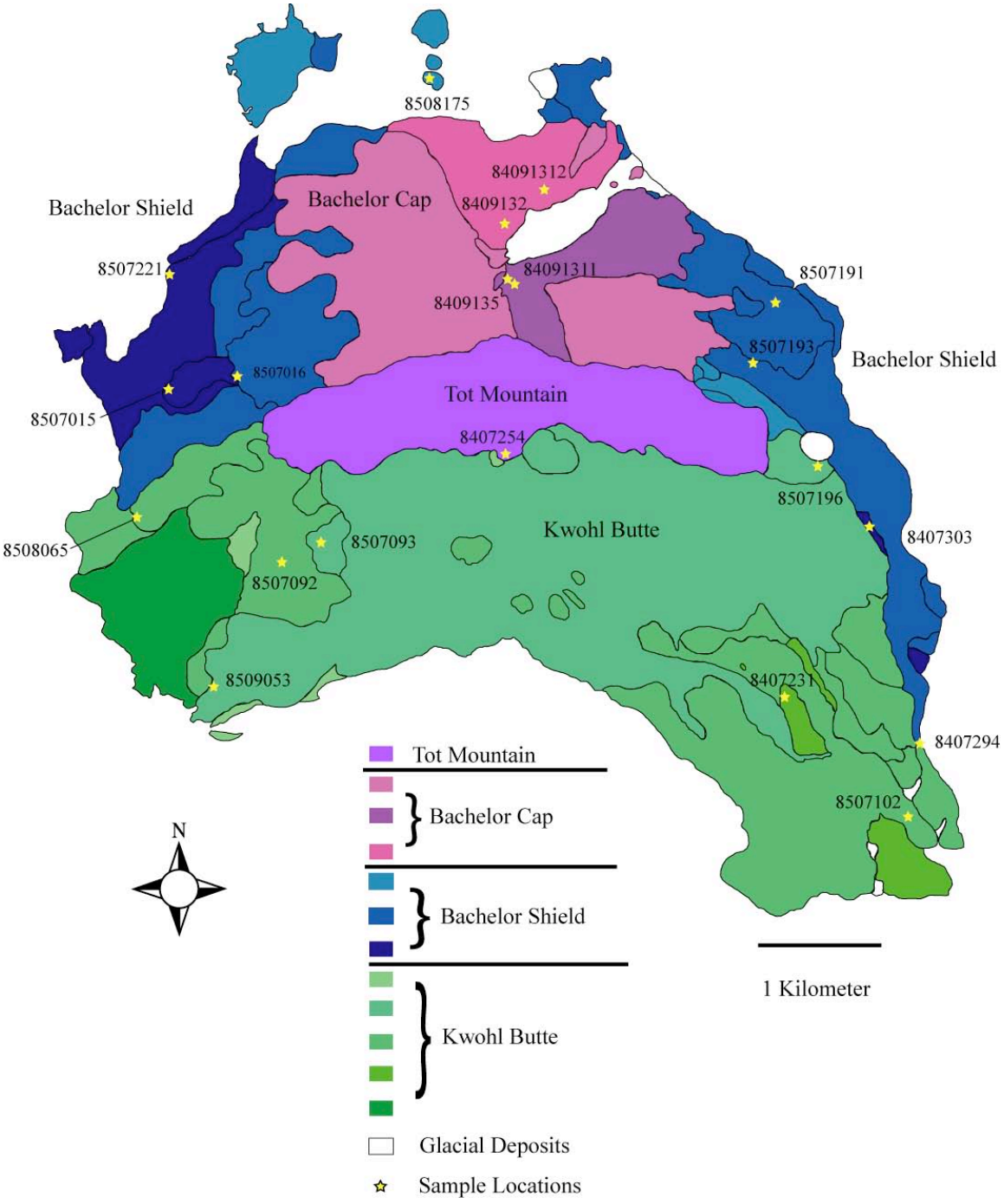

Figure 3. Geologic map of episode III of the MBVC. Shown are distinct eruptive units designated by color based on relative age of the lavas. The yellow stars indicate sample locations utilized for this study (modified from Scott and Gardner, 1992; Gardner, 1994b).

processes, such as fractionation of crystals from the remaining liquid, account for a significant portion of chemical diversity in erupted lavas. More commonly, however, open-system processes, such as assimilation of wallrock melt and replenishment by intrusion of more primitive magmas (Spera and Bohrson, 2001), contribute to the chemical and physical diversity. Bowen (1928) recognized a connection between latent heat released during crystal fractionation and the subsequent rise in wallrock temperatures, thus leading to increased potential for assimilation of wallrock. This observation helped foster conceptual understanding of the complex thermal and chemical interactions that occur between magma chambers and the country rock in which they reside.

The impact of open-system processes can be assessed through analysis of trace-element concentrations, radiogenic and stable isotope ratios, and textural and compositional changes in individual crystals within volcanic products. Typically, trace element trends will reflect removal of the minerals that are fractionated. For example, Sr is compatible in the Ca site within the crystal lattice of minerals such as plagioclase feldspar, and thus, relative depletion of Sr in a whole-rock analysis may suggest fractionation of plagioclase feldspar from a basaltic magma. Relative enrichment trends suggest that the element is incompatible in the fractionating assemblage or may also represent a replenishment of magma through a magmatic recharge event.

Radiogenic isotope ratios can provide evidence for open- or closed-system processes, such as crystal fractionation, assimilation, or magma recharge. During crystal fractionation, radiogenic isotope ratios of crystals and residual melt, such as $^{87}Sr/^{86}Sr$,

remain constant, provided the fractionation event is short-lived relative to the half-life of the parent isotope. An addition of material, either through assimilation of wallrock or intrusion and mixing of a more mafic magma, can alter the isotopic ratios of the initial magma (Faure and Mensing, 2005; Ramos and Reid, 2005; Zellmer et al., 2005). This modification can potentially be used to distinguish between an addition of crustal or mantle material. Mantle material typically has lower $^{87}Sr/^{86}Sr$ signatures, compared to continental crust, particularly upper crust. However, the isotope characteristics of the crust are dependent on the location and/or age. ^{87}Sr is a daughter product of ^{87}Rb, and the isotopic ratio of $^{87}Sr/^{86}Sr$ is influenced by the amount of rubidium found in the rock. Lavas that are more primitive have a stronger mantle signature and are typically formed deeper in the crust (Ramos and Reid, 2005). Radiogenic isotope ratios measured at the crystal scale (i.e., single crystal analyses) reflect magma conditions during the formation of crystals. Radiogenic isotope analysis of whole-rocks is an integration of all components of a lava, including the total crystal population. Analysis of whole-rocks can therefore mask variations between the crystal and the residual melt formed just prior to or during eruption. Analysis of individual crystals can reveal this masked isotope variation. Differences between the whole-rock and crystal isotope ratios provide evidence for open-system processes occurring during crystal formation.

Similarly, major and trace element compositions and textures of crystals can reflect petrogenetic processes. Plagioclase feldspar is a commonly used mineral in petrogenetic studies because the crystal grows in zonal patterns that can record both chemical and physical changes during the evolution of the magma, and it tends to be slow

to reequilibrate with the magma chamber (Tepley et al., 1999; Ginibre et al., 2007). These changes can record chemical differences caused by an influx of more primitive magma, such as in a recharge event, or a contamination by a more evolved material. Textural changes can also record physical changes within the magma chamber; for instance, resorption surfaces along crystal boundaries may indicate that areas of the crystal have been melted. By analyzing these chemical and textural changes in plagioclase feldspar, evidence can be provided in order to assess the relative importance of open- versus closed-system processes.

Mount Bachelor Magmatism

It has been proposed by several researchers (Hughes and Taylor, 1986; Tanton et al., 2001; Leeman et al., 2005) that rifting and extension along the central Oregon High Cascades has allowed the tapping of deeper, more primitive magmatic sources, thus leading to more mafic volcanism in this part of the Cascades. In order to understand the impact of the tectonic extension in this area, the magmatic processes (magma mixing, crystal fractionation, and assimilation) and the components that are involved in the generation of these lavas must be assessed. Ramos and Conrey (pers. comm., 2006) proposed to use microanalytical techniques to analyze Sr and Nd isotopic ratios on rocks from the MBVC. They hypothesize that these techniques will allow them to document the degree of isotopic disequilibrium and evaluate evidence for heterogeneous mantle sources. They proposed analysis of whole-rock and single grain isotope ratios in order to evaluate magmatic evolution of the MBVC. This study adopts the microanalytical

techniques of Ramos and Conrey (pers. comm., 2006) for episode III. The resulting data can be used for continued study in the active Cascade arc.

Understanding isotopic variability may shed light on the magmatic processes affecting the magma chamber(s) in the MBVC, including evidence for possible crustal contamination (Ramos and Reid, 2005; Ramos et al., 2005). Preliminary results have shown isotopic disequilibrium between the units of the MBVC (Ramos and Conrey, pers. comm., 2006). Preliminary evidence as presented by Gardner (1994b) suggests that most of the basaltic andesite of the MBVC was derived from basalt by crystal fractionation. She suggested the possibility of open-system magma mixing or assimilation in order to derive three distinct magma types observed at the MBVC. Her work did not examine radiogenic isotopes, which could provide additional insight on open-system processes. Examining isotopic ratio variability in units from episode III will allow an assessment of the importance of open- versus closed-system magmatic processes within a specific episode, thus providing a clearer picture of magmatism during one period of eruptive activity at the MBVC and the central Oregon High Cascades.

CHAPTER III

METHODS

Overview

Work by Gardner (1994b) provided a data set for an extensive suite of lavas spanning the entirety of the MBVC (see Data File A). Initial hypotheses concerning the magmatic processes during the formation of this volcanic chain were formulated based on these data. Work presented here was designed to build on the Gardner work. Episode III includes four units: Kwohl Butte, Bachelor Shield, Bachelor Cap, and Tot Mountain. An estimated 25 km^3 of material was erupted during the approximately 1,000 years of activity at these vents (Gardner, 1994b). This study focuses on two components: the whole-rock component, which includes all crystals and groundmass in a representative hand sample, and the plagioclase crystal component, which describes potential magmatic processes recorded during growth of these crystals. Textural and geochemical data obtained from petrography and ICP-MS, respectively, will provide insight into the evolution of the magma system. Similarly, $^{87}Sr/^{86}Sr$ and $^{143}Nd/^{144}Nd$ variations will document potential open-system processes that may have affected the magmatic system. Geochemical data and $^{87}Sr/^{86}Sr$ isotopic variation for individual plagioclase crystals will be used to evaluate the petrogenesis of the lavas of episode III at Mount Bachelor.

Sample Collection

The lavas composing the Mount Bachelor suite utilized in this study were obtained from the Cascades Volcano Observatory in February 2007. The samples were chosen to represent the diversity of location, age and composition of episode III.

Collected samples included seven from Kwohl Butte, eight from Bachelor Shield, four from Bachelor Cap, and one from Tot Mountain. The limited number of samples from Tot Mountain is a result of availability; because of difficulty in access, only one sample from this unit was collected during the initial mapping project (Gardner, 1994a). These samples have a wt % SiO_2 ranging between 50 and 56, and Mg numbers ranging from 44 to 63 (Gardner, 1994b). These geochemical ranges were used as a basis for sample collection as they are representative of the diversity in the lavas of episode III. Stratigraphic relationships among the samples were determined by using the sample map of Gardner (1994a).

Petrography

Six of the rock samples utilized for this study had accompanying thin sections. New thin sections were made of the remaining 14 samples. Approximately 3 cm × 1.5 cm billets were cut from the interior of the rock samples using a rock saw located at Central Washington University Department of Geology. Wagner Petrographic made the billets into standard thin sections. A petrographic microscope was used for analysis. Data, including crystal and groundmass textures, as well as modal composition, were compiled.

NDIC Microscopy

Five of the original 20 samples were selected for further analysis utilizing NDIC microscopy. These samples span all units of episode III and include two samples from Kwohl Butte, one sample from Bachelor Shield, one sample from Bachelor Cap and one sample from Tot Mountain. New billets were required for two of these samples. Wagner

Petrographic cut all billets to 150 μm thickness, and the sections were doubly polished. NDIC microscopy for this study was done at Portland State University under the direction of Dr. Martin Streck. The doubly polished thin sections were immersed for 25 to 30 s in concentrated fluoroboric (HBF_4) acid in order to preferentially dissolve Ca-rich zones (Tepley et al., 1999). The section was immediately removed from the acid and neutralized by immersion in a solution of sodium carbonate (Na_2CO_3), followed by rinsing with water (Anderson, 1983). This process results in calcic lows and sodic highs in plagioclase crystals, enabling microtopographic relief observable under reflected light microscopy (Anderson, 1983). The etched crystals were then carbon-coated to increase reflectivity and eliminate internal reflections (Pearce and Kolisnik, 1989). Parameters for carbon coating were set to 10-keV beam energy, 70 lbs of gas run on argon guns, and set on carbon impedance and density. The average thickness of the carbon coat is approximately 0.205 Å.

The NDIC images of the plagioclase crystals were taken using reflected light microscopy. NDIC microscopy uses reflected light in which a beam splitting technique enhances textural detail and crystal relief, thus revealing fine-scale zonal and discontinuous features within the crystal (Anderson, 1983). NDIC images were used to plan microprobe traverses. Between 7 and 11 plagioclase crystals for each 150-μm section were obtained for analysis on the electron microprobe, including microphenocrysts and phenocrysts.

Electron Microprobe

Plagioclase crystals imaged by NDIC were analyzed for major elements (e.g., Na, Ca) and the trace element Sr using the CAMECA SX-50 electron microprobe at Oregon State University under the direction of Dr. Frank Tepley. Calibration parameters included an accelerating potential of 15 kV, a beam current of 30 nA, between 10- and 40-s peak time, and a 1-µm-diameter spot size (Kohut and Nielson, 2003). Analyzed crystals were chosen based on textural complexities observed in NDIC images. Spot analyses from cores and rims were obtained from microphenocrysts and phenocrysts for three to seven crystals per 150-µm section. Traverses through complex crystal features were obtained for three to four crystals per 150-µm section. Traverse spacing varied from 5 to 14 µm, and data were collected using an autosampler. Analyses that were contaminated with groundmass or inclusions were excluded based on the MgO, FeO, and SiO_2 values. Finally, seven microlite cores were also analyzed. The anorthite (An), orthoclase (Or), and albite (Ab) atomic percents were calculated using equations 1 to 3:

$$\text{An \%} = \text{atomic ratio} \quad \frac{(Ca + Sr)}{(Ca + Sr + Na + K)} \times 100 \qquad (1)$$

$$\text{Or \%} = \text{atomic ratio} \quad \frac{K}{(Ca + Sr + Na + K)} \times 100 \qquad (2)$$

$$\text{Ab \%} = \text{atomic ratio} \quad \frac{Na}{(Ca + Sr + Na + K)} \times 100 \qquad (3)$$

The raw atomic percents for the selected elements were corrected for absorption and enhancement using the factors in Moore (1969).

Trace Element Analysis Using ICP-MS

Sample Preparation

Trace elements were determined at the GeoAnalytical Laboratory at Washington State University in Pullman, Washington. Twenty rock samples were ground using an iron bowl in a shatterbox swing mill (Knaack et al., 1994). Once ground, 2 g of the sample were mixed with 2 g of lithium tetraborate ($Li_2B_4O_7$) in a carbon crucible and placed in a muffle furnace set at 1,000 °C for 30 min to produce a fusion bead. The fusion bead was briefly ground in the shatterbox and 250 mg of powder was extracted and dissolved on a hotplate set at 110 °C in a Teflon vial using 6 ml of hydrofluoric (HF) acid, 2 ml of nitric (HNO_3) acid, and 2 ml of perchloric ($HClO_4$) acid (Crock and Lichte, 1982; Knaack et al., 1994). Once the solution was dried, an additional 2 ml of $HClO_4$ was added and evaporated at 165 °C. An additional 3 ml of HNO_3, 8 drops of hydrogen peroxide (H_2O_2), 5 drops of HF, and internal standards of In, Re, and Ru were then added to the samples (Knaack et al., 1994).

Instrument Operation and Calibration

All samples were analyzed on a HP 4500 ICP-MS. Samples were prepared using the methodology of Crock and Lichte, (1982), Lichte et al., (1987), and Knaack et al., (1994). Samples were loaded into the argon plasma at 1.0 ml/min with a peristaltic pump and automatic sampler. Each analysis was run in "multi-element" mode for a total count time of 5 s/element (Knaack et al., 1994). Issues related to isotope interferences were resolved by determining relative abundances. Sample and standard intensities were

downloaded and corrected for oxide and isobaric interferences using a spreadsheet and the internal standards In, Re, and Ru.

Radiogenic Isotope Analysis

Sample Preparation and Dissolution

Isotope analyses for 20 whole-rock samples and single crystals from two rock samples were utilized for this study. Whole-rock samples were ground using a tungsten carbide grinding box and an agate ball mill at Washington State University. Approximately 4 µg of whole-rock sample were weighed and added to cleaned Teflon beakers. Single crystals were collected from portions of two rock samples from Bachelor Cap (8409132) and Kwohl Butte (8507092). The rocks were broken using a hammer and plate mill grinder and sieved according to phi values 1,000 µm, 355 µm, 250 µm, and <250 µm. Samples of <355 µm and 250 µm were sonicated in water and separated using a Frantz magnetic separator. Plagioclase feldspar, olivine, and an unknown white material were handpicked. Thirteen plagioclase feldspar grains and four grains of olivine were obtained from sample 8409132 and eight plagioclase feldspar grains and two crystals of an unknown substance were obtained from sample 8507092. Crystal samples were weighed and placed into Teflon beakers.

Dissolution of both whole-rock and single grain samples occurred in the Central Washington University clean laboratory. Approximately 3 ml of HNO_3 acid and 6 ml of HF acid were added to each beaker containing the whole-rock samples. Lesser volumes (10 drops of HNO_3 and 20 drops of HF) were added to the single grain samples. The beakers were left on a hot plate for 12 hr at 100 to 120 °C. The lids were removed and

washed with 1 ml of water, and the beakers were left on the hotplate to evaporate the aqueous material. Approximately 10 ml for the whole-rock samples and 2 ml for the single grain samples of 1:1 HNO_3: H_2O acid were added to the beakers. The beakers were recovered and placed onto the hotplate for approximately 12 hr. Beaker lids were again removed, and the liquids were allowed to evaporate. Approximately 10 ml for the whole-rock samples and 5 ml for the single grain samples of 6 N hydrochloric (HCl) acid were added to the beakers. The beakers were covered and again placed on the hotplate for 12 hr. A small amount of 1:1 HNO_3: H_2O (approximately 2 ml) was added to the whole-rock sample beakers to coat the bottom and allowed to sit, cold, overnight.

The whole-rock sample solutions were placed into 50-ml centrifuge tubes and centrifuged for 10 min at 3,500 RPM. If residual solid material remained, the dissolution procedure was repeated until all material was dissolved. Once all material was dissolved, the samples were reweighed and one quarter of weighed material was removed and placed into cleaned Teflon beakers. The single grain sample solutions were visually inspected to ensure complete dissolution. All solutions were placed on the hotplate and evaporated completely. Whole-rock samples were then redissolved in 1 ml of 2.5 N HCL and single grain samples in 0.5 ml of 2.5 N HCl in preparation for cation exchange columns. The solutions were placed in 1.5-ml centrifuge tubes and centrifuged for 5 min at 3,000 RPM.

Column Chromatography

To obtain pure Sr and Nd samples, 20-ml quartz columns filled with cation exchange resin were used. Columns were prepared using 10 ml of 2.5 N HCl.

Centrifuged samples were then loaded onto individual columns using a 1,000-µl pipette. Samples were washed with 2.5 N HCl using six consecutive steps of volumes of 0.5 ml, 0.5 ml, 2 ml, 6.5 ml, 3 ml, 5 ml, 6 ml, respectively. Each next step was initiated after all the acid from the previous step had drained from the reservoir into the resin bed. All Sr was collected in the Teflon beakers used for digestion after cleaning. Columns were washed with 10 ml of 6 N HCl for REE separation; the elution was collected in cleaned Teflon beakers. REE were only collected for whole-rock samples. Finally, the cation exchange columns were washed with 15 ml of 6 N HCl for resin cleaning. Once the reservoirs were fully drained, the columns were backwashed with filtered water, which re-expanded the cation exchange resin. Once the Sr and REE were collected, the Teflon beakers containing these elements were placed on the hot plate and allowed to dry, leaving only a residue of Sr and REE in each respective beaker.

Once dried, 0.5 ml of 0.25 N HCl was added to the beakers containing the REE. Cation exchange columns using REE spec resin were prepared using 10 ml of 0.25 N HCl. The samples were then loaded onto individual columns using a 1,000-µl pipette. Samples were washed with 0.25 N HCl using five consecutive steps of volumes 0.5 ml, 0.5 ml, 1 ml, 4 ml, 6 ml, respectively. As with Sr elution, each next step was initiated after all the acid from the previous step had drained from the reservoir into the resin bed. All Nd was collected in cleaned Teflon beakers. Columns were washed with 15 ml of 6 N HCl for resin cleaning and 3 ml of 0.25 N HCl was added before storage. The Teflon beakers of Nd were placed on the hot plate and allowed to dry, leaving only a residue of

Nd. Once dry, Sr and Nd samples were ready for sample loading and analysis on the thermal ionization mass spectrometer (TIMS).

Sample Loading and Analysis

Sr samples were loaded onto Re filaments mounted on Cathodian beads. The dried whole-rock samples were dissolved in 3 drops of 5% HNO_3 and the single grain samples were dissolved in 2 µl of 5% HNO_3 acid. For both whole-rock and single grain samples, 1 µl of dissolved solution was loaded on the filaments, along with 1 µl of tantalum (TaO_2) acid and 1 µl of 5% phosphoric (H_3PO_4) acid to stabilize the ionization of the Sr. Samples were allowed to air dry for approximately 1 hr and fully dried by putting current through the filament (0.8 to 1.0 V to red glow). Once samples were dry, the Cathodian filaments were loaded into the turret and placed into the mass spectrometer. All samples were analyzed on a VG Sector 54-30 TIMS, located at Central Washington University under the supervision of Frank Ramos. Sr sample calibration to a standard (NBS 987) was conducted for each new turret. All standards fell within 0.00003 of each other. Sr samples were analyzed using five collectors in dynamic mode with $^{87}Sr/^{86}Sr$ normalized to $^{86}Sr/^{88}Sr = 0.1194$. The samples were analyzed for Sr mass 88 at a minimum intensity of 3×10^{-11} A.

Nd samples were loaded onto Re filaments on one side of a triple filament assembly. Samples were dissolved in 3 drops of 5% HNO_3 and 1 µl of sample was loaded. Samples were allowed to dry for approximately 1 hr. Once samples were dry, the Re filaments were loaded into the turret and placed in the mass spectrometer. Nd samples were analyzed on the Central Washington University VG Sector 54-30. Sample

calibration to a standard (JNdi-1) was conducted for each new turret. All standards fell within 0.00001 of each other. Nd samples were analyzed using seven collectors that were calibrated to each other using Nd mass 144 at a minimum of 5×10^{-12} A.

CHAPTER IV

RESULTS

Sample Locations and Descriptions

Twenty lavas erupted over the span of episode III were the focus for this study. Cynthia Gardner and Willie Scott collected all samples during 1984 and 1985. For this study, samples used are as follows: eight samples from Kwohl Butte, seven samples from Bachelor Shield, four samples from the Bachelor Cap and one sample from Tot Mountain. Sample locations are presented in Figure 3. All samples are henceforth described in the stratigraphic order as described by Data File A, which includes all oxide and XRF (x-ray florescence) data, published in Gardner (1994b), as well as the ICP-MS and radiogenic isotope data collected as part of this study.

Hand samples range from medium to dark gray. Most are marginally to highly porphyritic, with phenocryst abundances ranging from 30% to 50%. All samples contain plagioclase feldspar, and in some samples, larger phenocrysts of olivine are present (Table 1). Only in Bachelor Cap and Tot Mountain is there any observable clinopyroxene. In these cases, the clinopyroxene occurs as small (<1 mm) crystals. A few samples show signs of weathering, including sample 84091311 from Bachelor Cap that has one crystal that has apparently been oxidized. Most samples are vesiculated, although some show only small vesicles in thin section (see Table 1).

Petrography

Samples from the units composing episode III are mineralogically variable, but all samples contain plagioclase feldspar and olivine crystals. Modal abundances of

TABLE 1. MODAL ABUNDANCES AND ROCK TYPES

Sample	Plagioclase (%)	Olivine (%)	Ground -mass (%)	Groundmass mineralogy†	Vesicle (%)	Rock type‡
Tot Mountain§						
8407254	45	24	30	pl>ox>ol>cpx	30	BA
Bachelor Cap						
84091312	45	15	40	gl>pl=ox>ol/cpx	25	BA
8409132	40	30	30	gl=pl>ol=ox/cpx	30	BA
8409135	50	20	30	ox=gl>ol/pl±cpx	10	BA
84091311	45	25	30	pl>gl>ox>ol/cpx	15	BA
Bachelor Shield						
8408175	20	25	55	gl>pl>ol=ox/	7	B
8507016	25	10	65	pl=gl>ol=ox	10	BA
8507193	45	30	25	pl>ol=ox	20	BA
8507191	40	10	50	gl>pl>ol=ox	15	BA
8407294	50	20	30	pl>ol>ox	7	BA
8407303	50	20	30	ox>pl=ol	10	B
8507015	50	30	20	pl>ol>gl=ox	3	B
8507221	35	25	40	pl>ol>ox>gl	7	B
Kwohl Butte						
8509053	35	15	50	gl>pl>ol>ox	15	BA
8507196	40	35	25	pl>ol>ox±cpx	10	BA
8507093	50	20	30	pl=gl>ol>gl	20	BA
8507092	50	20	30	pl>ol>ox>gl	1	B
8507102	40	20	40	pl=gl>ol>ox	3	B
8408065	40	20	40	pl>ol=ox	7	B
8407231	50	10	40	pl>gl/ox>ol/id	1	BA

† Tot Mountain (sample 8407254) modal abundance includes 1% clinopyroxene.

‡ Groundmass mineralogy includes plagioclase feldspar (pl), glass (gl), oxides (ox), olivine (ol), and clinopyroxene (cpx). Modal abundances are on vesicle free basis.

§ Rock types include basalt (B) and basaltic-andesite (BA).

plagioclase feldspar and olivine microphenocrysts and phenocrysts, along with groundmass abundance and mineralogy are presented in Table 1. All modal abundances are normalized on a vesicle-free basis. The textures observed by the petrographic analyses show a general distinction between the older units and younger units, including

Kwohl Butte (Figure 4) and Bachelor Shield (Figure 5) and the younger units, Bachelor Cap (Figure 6) and Tot Mountain (Figure 7). The older units tend to have a distinction in size between the phenocrysts and microphenocrysts and the groundmass. The younger units show a gradual decrease in size from phenocrysts to groundmass.

Kwohl Butte, the oldest unit of episode III, shows distinctions between older and younger lava flows. Of the seven representative lavas, three are basalts (SiO_2 ranges from 50.3 to 50.6 wt %) whereas the remaining four are basaltic-andesites (SiO_2 ranges from 52.2 to 53.8 wt %). The earliest erupted lavas show mostly fine-grained

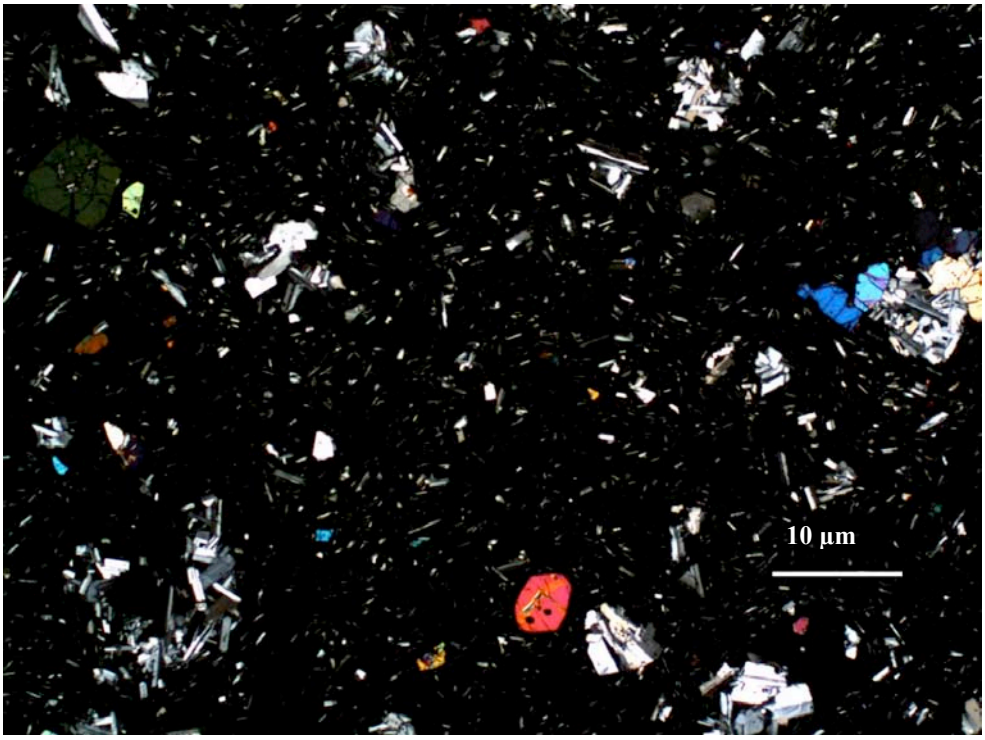

Figure 4. Petrographic image of Kwohl Butte lava (sample 8509053).

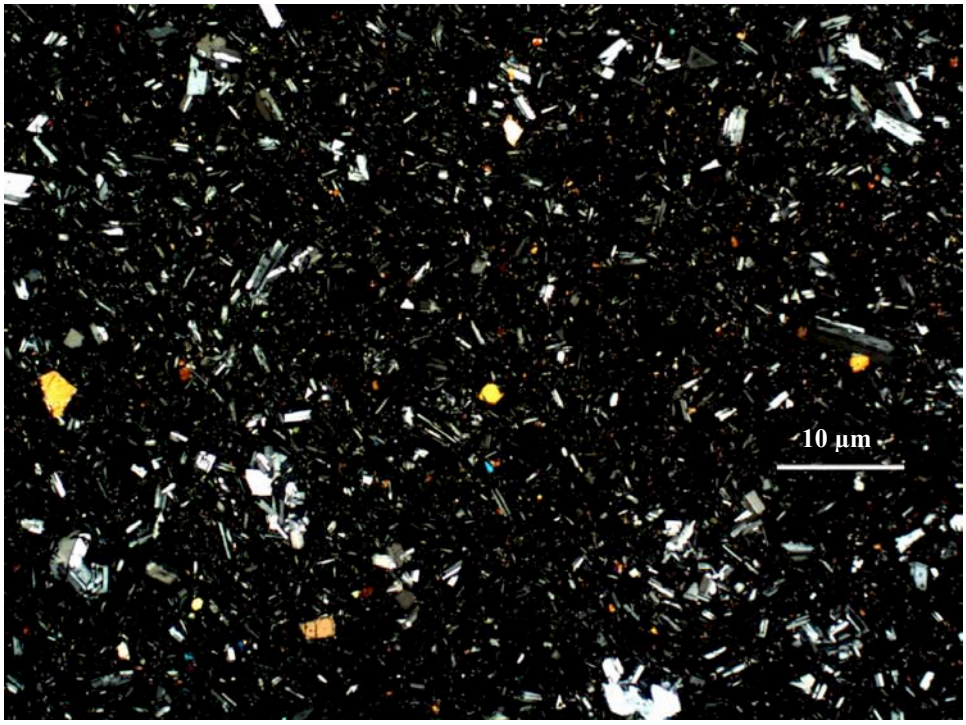

Figure 5. Petrographic image of Bachelor Shield lava (sample 8507016).

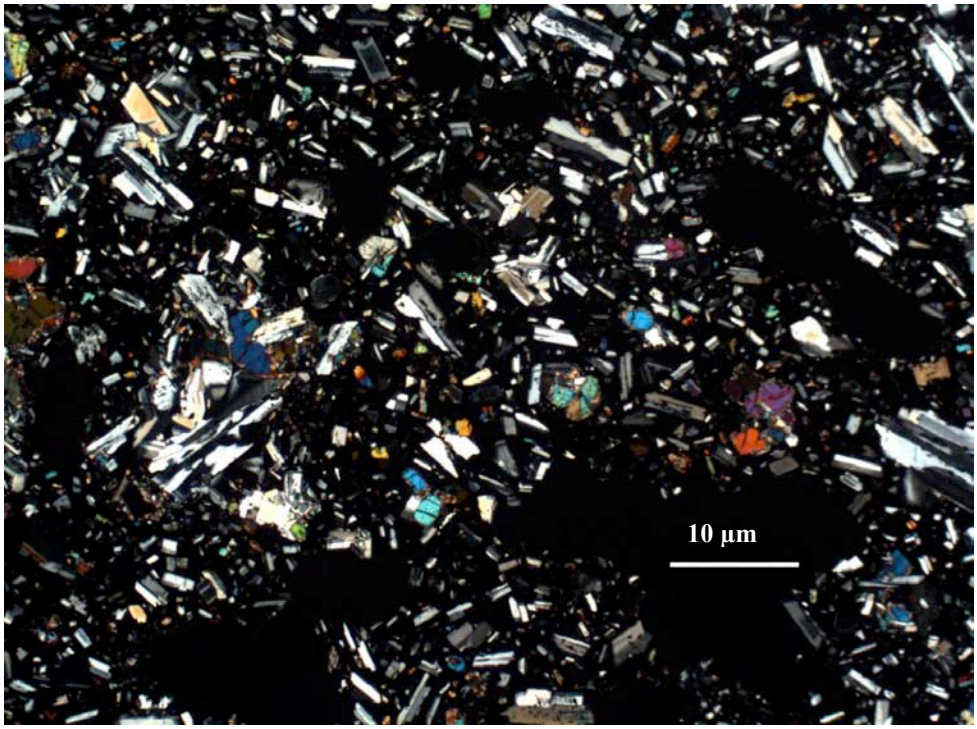

Figure 6. Petrographic image of Bachelor Cap lava (sample 8409132).

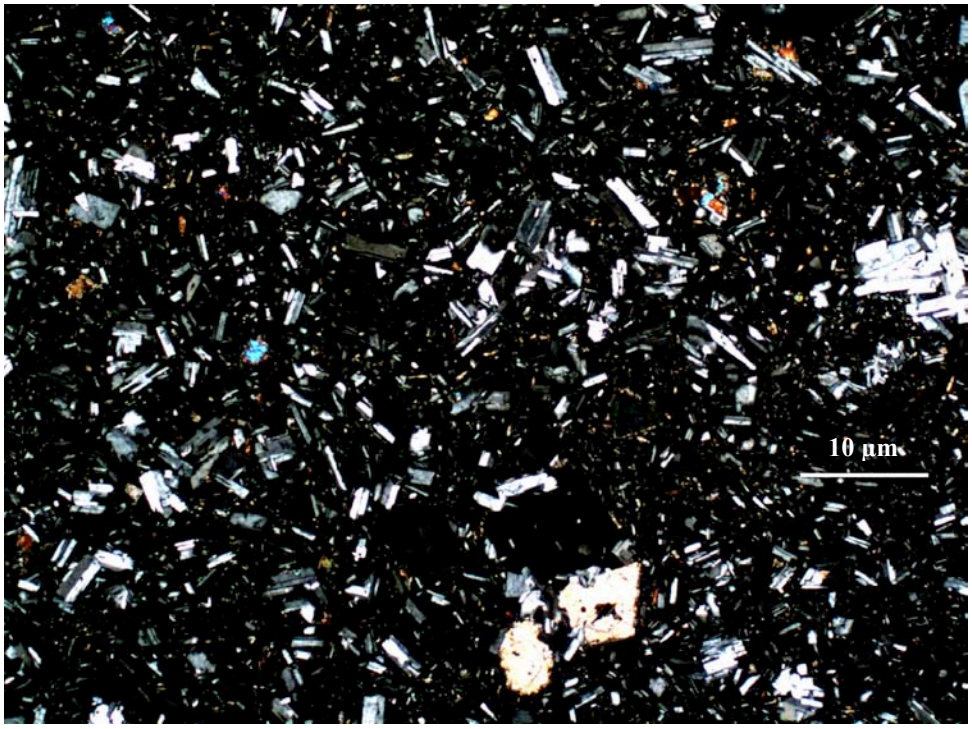

Figure 7. Petrographic image of Tot Mountain lava (sample 8407254).

groundmass dominated by plagioclase feldspar and/or glass. Some of these early flows are characterized by trachytic texture. The early lavas of Kwohl Butte are dominated by olivine, the only exception being the oldest sample (8407231). Olivine crystals are typically present as phenocrysts and within the groundmass. Olivine is observed as inclusions in plagioclase feldspar phenocrysts in all samples. An increase in grain size occurs with plagioclase feldspar becoming the dominant phenocryst phase in the younger lavas (8507093) to the older samples from Kwohl Butte (8509053). Plagioclase phenocrysts are typically subhedral, with crystals averaging 1 mm in size. Oscillatory zoning, glomeroporphyritic and sieve textures are observed in all Kwohl Butte plagioclase feldspar phenocrysts. Groundmass mineralogy includes plagioclase feldspar, some forming trachytic texture, olivine, and in some circumstances, glass.

The middle unit of episode III consists of the Bachelor shield, which includes the lavas on the periphery of the main butte. Of these eight lavas, four are basalts (SiO_2 ranges from 50.8 to 51.6 wt %) and four are basaltic andesites (SiO_2 ranges from 53.0 to 53.9 wt %). The lavas of the Bachelor Shield are porphyritic with few large phenocrysts. The modal abundance for plagioclase feldspar microphenocrysts and phenocrysts ranges from 20% to 50%. Variations in the groundmass assemblages exist between the lavas, but most have plagioclase feldspar as the dominant phase. Plagioclase feldspar phenocrysts of the Bachelor Shield range from subhedral to euhedral laths with some acicular phenocrysts. Crystals are typically between 1 and 1.5 mm in size. Crystals tend to have oscillatory zoning and sieve textures, some to a very high degree. Olivine crystals exist as both phenocrysts and groundmass crystals. The largest olivine phenocryst is 3 mm, whereas most range between 1 and 2 mm. Olivine crystals are conchoidally fractured. Groundmass mineralogy in samples from the Bachelor Shield is typically dominated by plagioclase feldspar; in some cases exhibiting trachytic textures. Glass and vesicles are also present in most samples; some samples have diktytaxitic textures.

The final unit of episode III consists of both Bachelor Cap and Tot Mountain. All lavas of this unit are basaltic andesite (SiO_2 ranges from 55.8 to 56.9 wt %) and are comprised of large phenocrysts of both plagioclase feldspar and olivine, although plagioclase feldspar is dominant. Groundmass ranges from 30% to 40% modal abundance and glass and/or oxides are the dominant phases. This unit also has minor amounts of clinopyroxene in the groundmass and as phenocrysts (<1% modal

abundance). Plagioclase feldspar phenocrysts of the Bachelor Cap are mostly subhedral to anhedral laths, ranging in size from 1 to 2.5 mm. Most phenocrysts are glomeroporphyritic, some creating rosettes. Complex textures, such as oscillatory zoning and sieve textures, are not common. Most plagioclase feldspar crystals are highly altered. Olivine crystals exist as both phenocrysts and as groundmass crystals. Most crystals have reaction rims. Olivine also exists as inclusions in plagioclase feldspar phenocrysts. Groundmass for Bachelor Cap samples includes plagioclase feldspar, olivine, glass and minor amounts of clinopyroxene.

The sample from Tot Mountain is comprised of subhedral to anhedral plagioclase feldspar phenocrysts that range in size from 1 to 2 mm. Oscillatory zoning is observed in some crystals. Phenocrysts of clinopyroxene are also present, typically 1 mm or less in size. Olivine crystals exist as both phenocrysts and in groundmass and have reaction rims. Some olivine crystals exist as inclusions within plagioclase feldspar crystals. Groundmass includes plagioclase feldspar, olivine, and clinopyroxene.

NDIC Imaging

A total of 55 NDIC images were captured; of these, 46 images were used for this study. The breakdown of crystals imaged by NDIC is provided in Table 2.

TABLE 2. TOTAL NUMBER OF CRYSTALS IMAGED BY NDIC MICROSCOPY

Sample	mph	Ph	Total crystals
8407254 (Tot Mountain)	5	6	11
8409132 (Bachelor Cap)	4	5	9
8407294 (Bachelor Shield)	6	5	11
8509053 (Kwohl Butte)	2	5	7
8507092 (Kwohl Butte)	4	4	8

Notes: mph—microphenocrysts; ph—phenocrysts.

The NDIC microscopy images were used to capture the textural features of individual plagioclase feldspar crystals from selected 150-µm sections, including samples 8507092 and 8509053 from Kwohl Butte, sample 8407294 from Bachelor Shield, sample 8409132 from Bachelor Cap, and sample 8407254 from Tot Mountain. The NDIC images were separated into three textural categories: simple textures (ST), intermediate textures (IT), and complex textures (CT). ST crystals are characterized by oscillatory zoning; sieve textures are rare. Figure 8 illustrates an example of a typical ST crystal

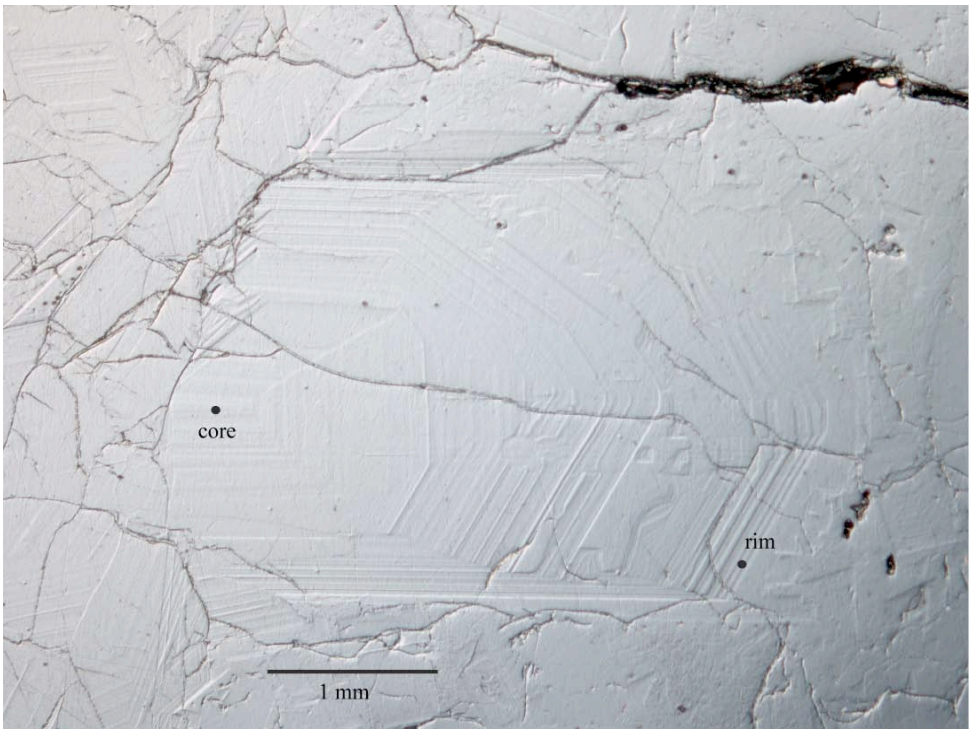

Figure 8. NDIC image of crystal 8409132_p3. This figure illustrates an example of ST.

from the Bachelor Cap, sample and crystal number 8409132_p3. IT crystals are characterized by disequilibrium textures, either areas of resorption or crystal areas that have undergone partial melting, thus resulting in minor sieved zones. The crystals included in the intermediate category tend to have oscillatory zoning. Figure 9 illustrates

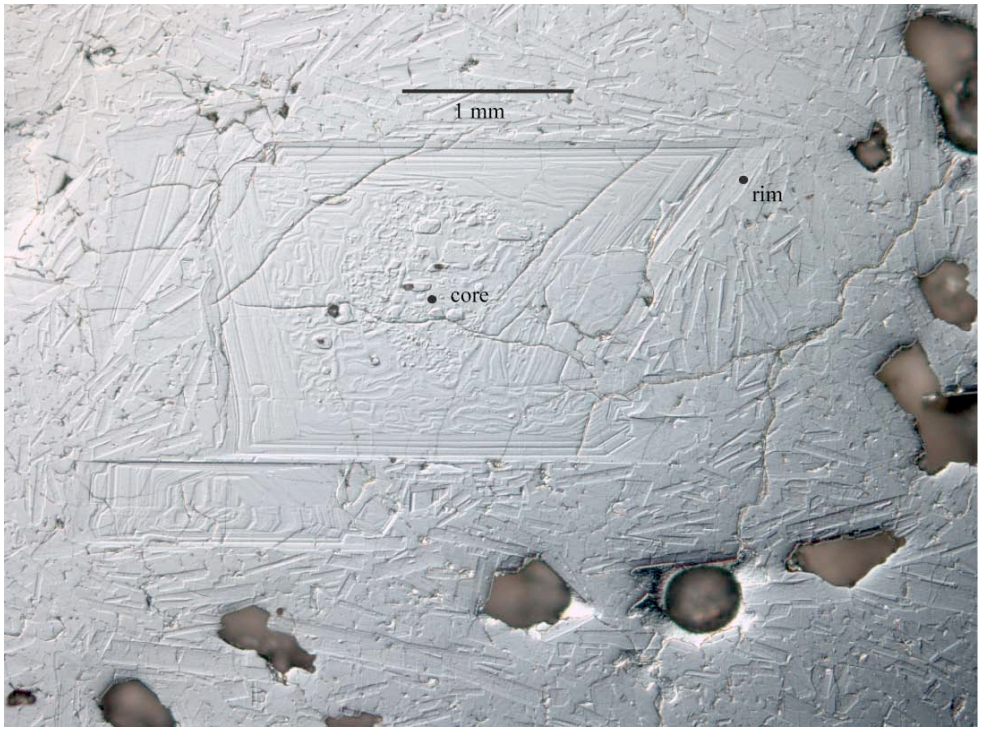

Figure 9. NDIC image of crystal 8509053_p3. This figure illustrates an example of IT. one example of a crystal that has experienced some degree of textural disequilibrium. Crystal 8509053_p3 shows areas of sieving, as well as areas that may have undergone a small degree of resorption. Finally, CT crystals are those crystals in which textural disequilibrium is definitely apparent. Most crystals in this category are strongly sieved, and some show areas of resorption. Figure 10 illustrates an example of crystal 8507092_p2 that has a heavily sieved core. Oscillatory zoning is still observable, but only in the rim of this crystal. The NDIC images of crystals in which cores and rims were analyzed are compiled in Data Files B–D.

Electron Microprobe

A subset of crystals imaged by NDIC were analyzed for major and selected trace elements to determine the range of compositions present in the samples and assess

Figure 10. NDIC image of crystal 8407092_p2. This figure illustrates an example of CT. compositional changes in the context of texture. Eighty-one crystals were selected for analysis on the electron microprobe. Single point analyses at cores and rims for 27 selected microphenocrysts and phenocrysts, traverses from core to rims on the remaining 19 microphenocrysts and phenocrysts, and single points on microlites were included in the study. Table 3 combines core and rim and traverse data. Major elements, including Na, Fe, Ca, K, Ti, Si, Al, Mg, O and the trace element Sr, are reported.

Core and Rim Analyses

Data were collected for cores and rims of all crystals sampled. Crystal textures and electron microprobe data are compiled in Data Files E–I. An, Or and Ab contents were calculated as previously stated, averaged and one standard deviation was

TABLE 3. TOTAL NUMBER OF CRYSTALS ANALYZED BY ELECTRON MICROPROBE

Sample	ml	mph	ph	Total
8407254 (Tot Mountain)	7	5	6	18
8409132 (Bachelor Cap)	7	4	5	16
8407294 (Bachelor Shield)	7	6	5	18
8509053 (Kwohl Butte)	7	2	5	14
8507092 (Kwohl Butte)	7	4	4	15

Notes: ml—microlites; mph—microphenocrysts; ph—phenocrysts.

determined. Table 4 shows the average and one standard deviation data for all core and rim analyses (including core and rim data from traversed crystals).

TABLE 4. AVERAGE ANORTHITE, ORTHOCLASE, AND ALBITE COMPOSITIONS FOR CORE AND RIM ANALYSES

Sample	Area analyzed	An ± 1σ	Or ± 1σ	Ab ± 1σ
Tot Mountain				
8407254	Core	75.20 ± 8.4	0.54 ± 0.3	24.26 ± 8.1
8407254	Rim	55.09 ± 6.8	1.65 ± 0.5	43.26 ± 6.3
Bachelor Cap				
8409132	Core	76.68 ± 3.7	0.52 ± 0.1	22.81 ± 3.6
8409132	Rim	58.08 ± 19.0	1.83 ± 1.6	40.09 ± 17.5
Bachelor Shield				
8407294	Core	77.13 ± 3.3	0.48 ± 0.1	22.39 ± 3.2
8407294	Rim	68.49 ± 9.4	0.98 ± 0.5	30.53 ± 8.9
Kwohl Butte				
8509053	Core	79.05 ± 3.8	0.53 ± 0.2	20.42 ± 3.8
8509053	Rim	67.89 ± 7.4	0.92 ± 0.4	31.18 ± 7.1
Kwohl Butte				
8507092	Core	69.24 ± 8.4	1.08 ± 0.6	29.68 ± 7.9
8507092	Rim	61.54 ± 9.0	1.62 ± 0.7	38.85 ± 8.4

Notes: An—anorthite; Or—orthoclase; Ab—albite.

General trends are observed, namely the higher average An content observed in the cores compared to the rims for all samples. Samples fall between An_{55} to An_{77},

ranging from labradorite (An_{50-70}) to bytownite (An_{70-90}). The younger lavas, including samples from Bachelor Cap and Tot Mountain, show very similar averages for An and Ab end members. Graphs illustrating the anorthite contents for microphenocrysts and phenocrysts for all five samples are compiled in Data File J.

Traverse Analyses

Traverses on three or four crystals per sample were completed. Eighteen to 50 points along a given traverse were collected. Variation on the number of collected points depended on the length of the crystal. The spacing between each collected point ranged from 6 μm to 14 μm. Traverse lengths along the crystal range from 63 μm to 410 μm. Major and trace elements are recorded in Data Files E–I. An, Or, and Ab contents were calculated, averaged and the standard deviations were determined. These values are expressed in Table 5.

All averages fall between An_{55} to An_{79}, again ranging between labradorite and bytownite in composition. A selected number of NDIC images showing An contents versus distance are presented in Figures 11 through 15. The remaining anorthite trends and the accompanying NDIC images can be found in Data File K. The anorthite content for all samples typically varies from core to rim in all crystals, indicative of the growth of plagioclase feldspar crystal. Oscillatory zoning is defined by Haase et al. (1980) as a change between 5 and 15 mol % over 10 to 20 μm. The above results show that the majority of the changes observed in the Bachelor lavas are within 10 mol %, suggesting that the anorthite trends are associated with oscillatory zoning. A general decrease in anorthite near the rim of the crystal is observed for a majority of the crystals. A good

TABLE 5. AVERAGE ANORTHITE, ORTHOCLASE, AND ALBITE COMPOSITIONS FOR CRYSTAL TRAVERSES

Episode III unit and crystal number	An ± 1σ	Or ± 1σ	Ab ± 1σ
Tot Mountain			
8407254_1	78.89 ± 3.9	0.46 ± 0.2	20.66 ± 3.7
8407254_2	73.45 ± 8.6	0.61 ± 0.4	25.89 ± 8.2
8407254_3	63.71 ± 5.5	1.08 ± 0.6	35.21 ± 5.0
8407254_4	63.71 ± 5.5	1.08 ± 0.6	35.21 ± 5.0
Bachelor Cap			
8409132_1	76.21 ± 2.3	0.50 ± 0.1	23.29 ± 2.2
8409132_2	75.17 ± 3.3	0.58 ± 0.1	24.26 ± 3.2
8409132_3	72.29 ± 11.5	0.78 ± 0.7	26.93 ± 10.8
8409132_4	78.76 ± 4.8	0.52 ± 0.3	20.72 ± 4.6
Bachelor Shield			
8407294_1	73.81 ± 10.4	0.74 ± 0.7	25.45 ± 9.8
8407294_2	72.95 ± 4.1	0.67 ± 0.2	26.38 ± 3.9
8407294_3	76.74 ± 4.3	0.56 ± 0.1	22.70 ± 4.2
8407294_4	72.24 ± 5.9	0.72 ± 0.3	27.05 ± 5.6
Kwohl Butte			
8509053_1	75.74 ± 3.9	0.55 ± 0.1	23.71 ± 3.8
8509053_2	76.82 ± 5.8	0.52 ± 0.2	22.66 ± 5.6
8509053_3	74.25 ± 3.9	0.61 ± 0.2	25.14 ± 3.8
Kwohl Butte			
8507092_1	55.40 ± 9.0	2.36 ± 1.5	42.24 ± 7.5
8507092_2	71.23 ± 7.1	0.86 ± 0.5	27.91 ± 6.6
8507092_3	74.82 ± 8.2	0.73 ± 0.5	24.46 ± 7.8
8507092_4	74.93 ± 5.3	0.75 ± 0.4	24.32 ± 5.0

Notes: An—anorthite; Or—orthoclase; Ab—albite.

A

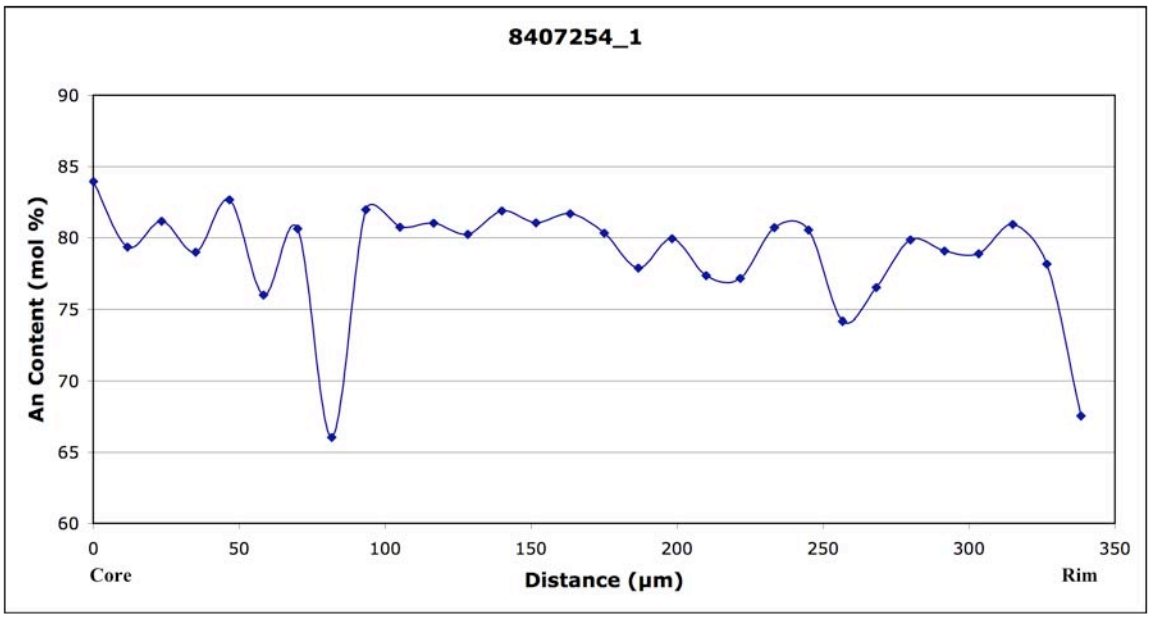

B

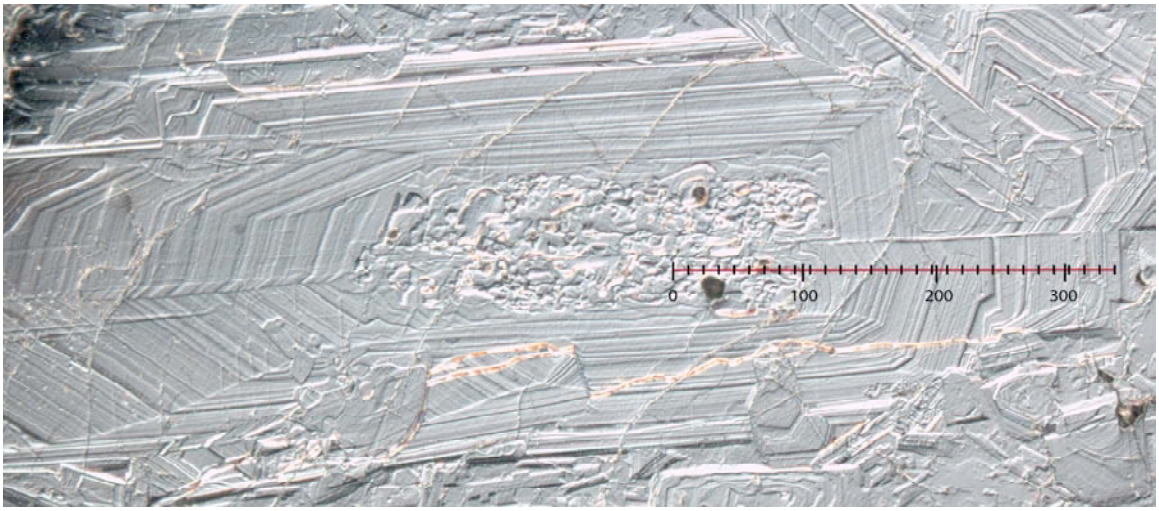

Figure 11. Anorthite content across a traverse for Tot Mountain (sample 8407254). A) An content (mol %) plotted versus distance from core to rim of sample. B) Nomarski differential interference contrast image of crystal with microprobe traverse plotted for reference. Crystal is classified as CT.

A

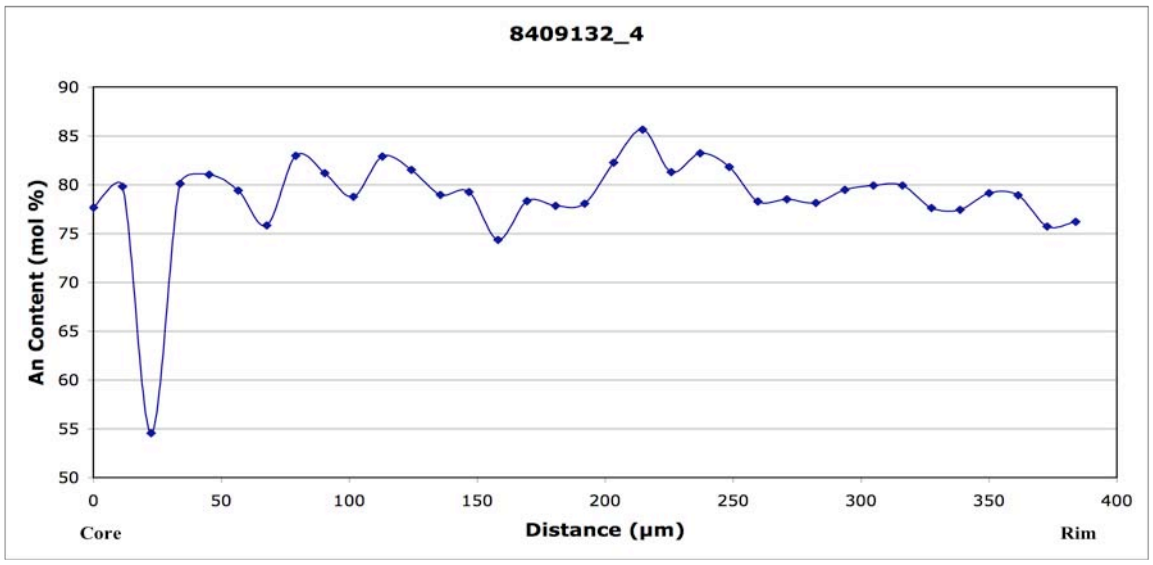

B

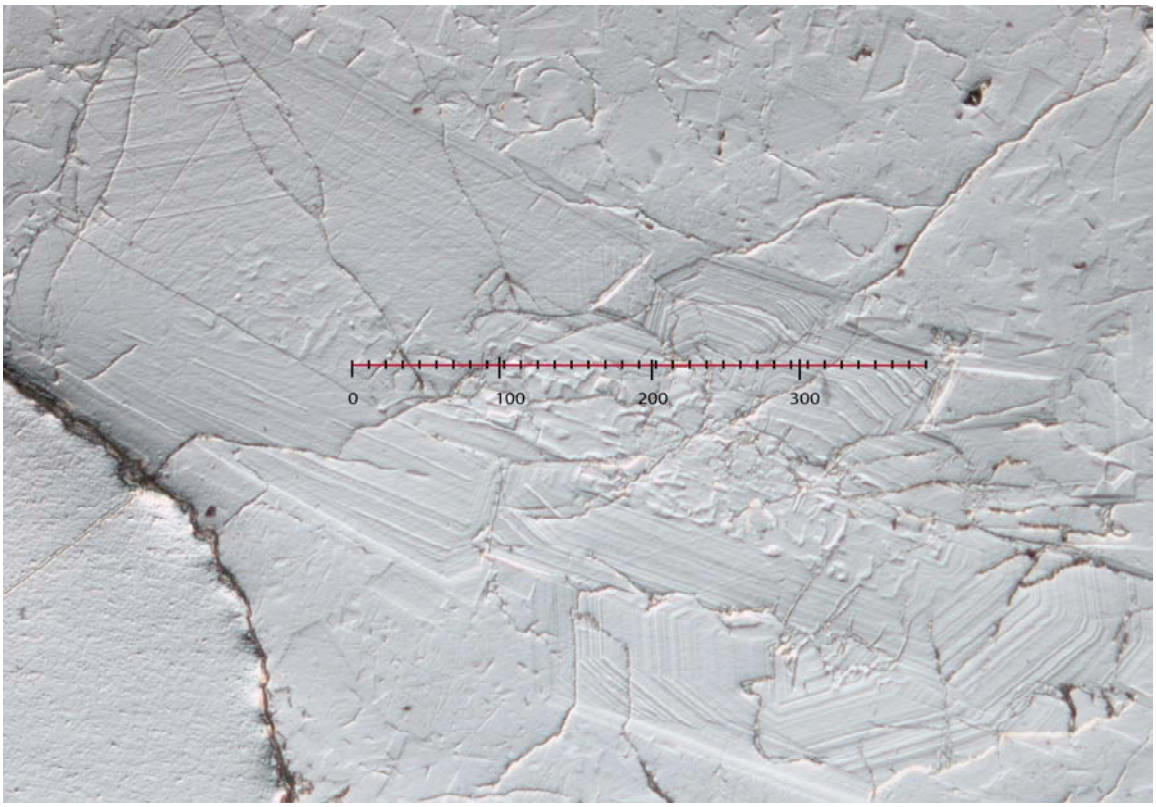

Figure 12. Anorthite content across a traverse for Bachelor Cap (sample 8409132). A) An content (mol %) plotted versus distance from core to rim of sample. B) Nomarski differential interference contrast image of crystal with microprobe traverse plotted for reference. Crystal is classified as IT.

A

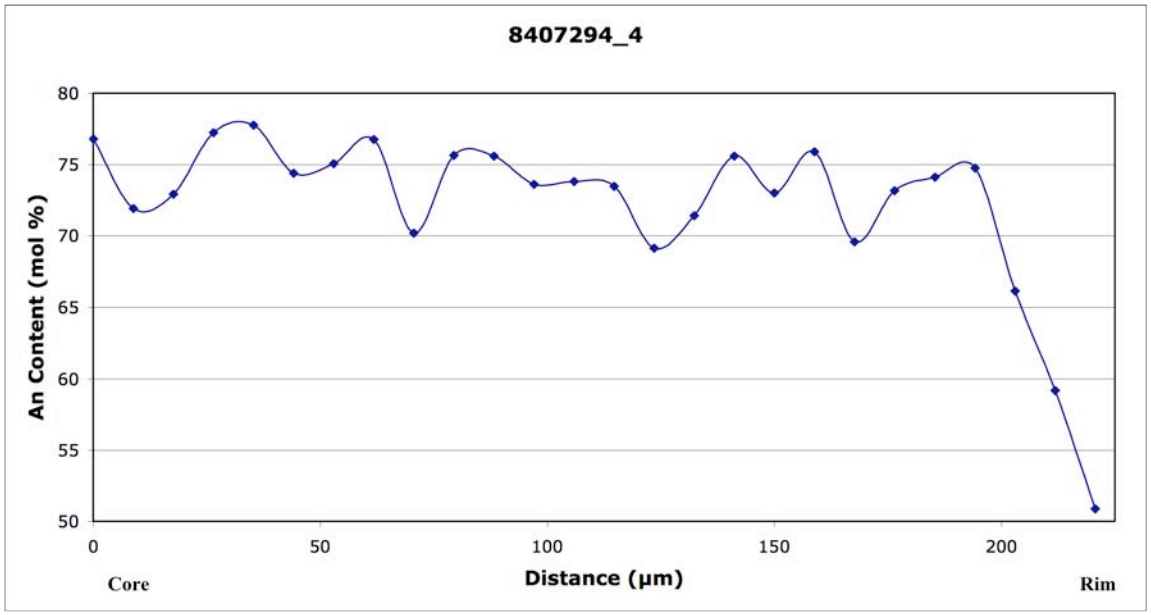

B

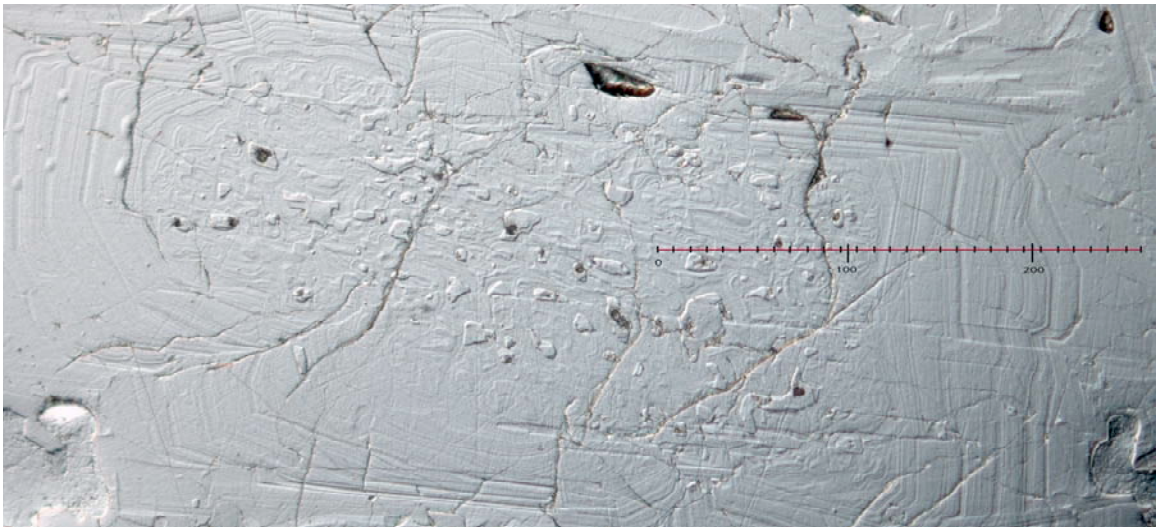

Figure 13. Anorthite content across a traverse for Bachelor Shield (sample 8407294). A) An content (mol %) plotted versus distance from core to rim of sample. B) Nomarski differential interference contrast image of crystal with microprobe traverse plotted for reference. Crystal is classified as CT.

A

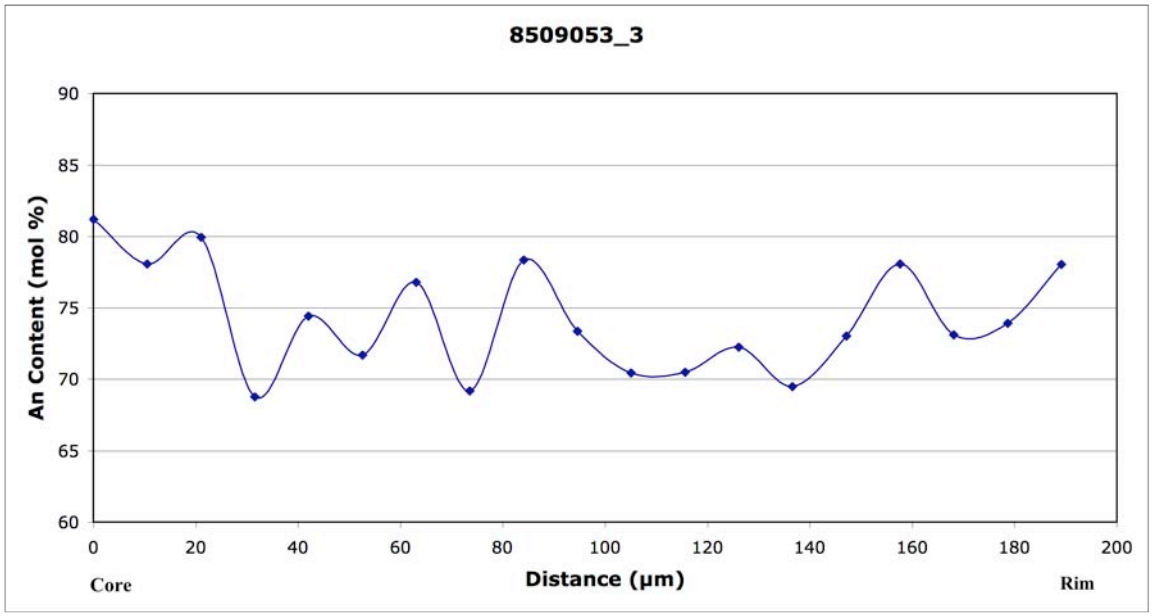

B

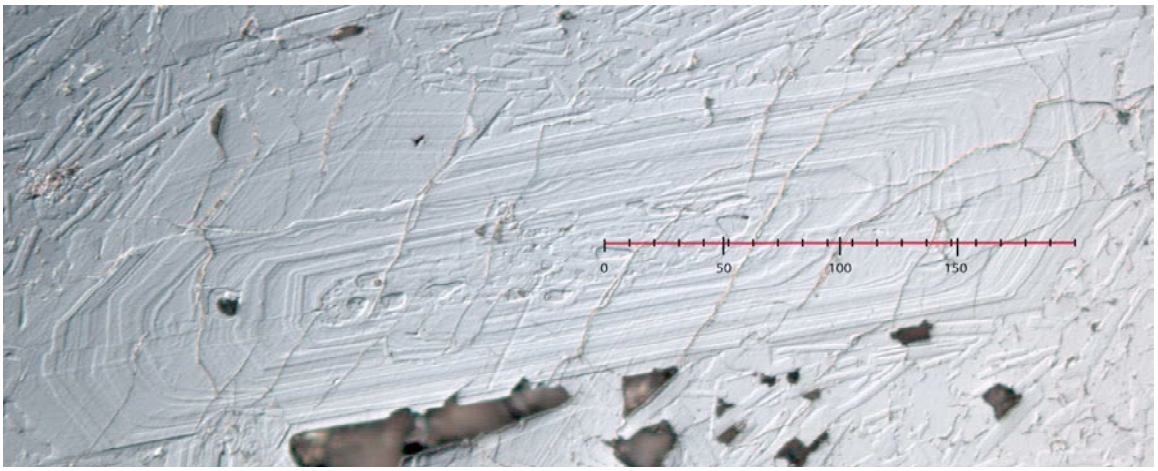

Figure 14. Anorthite content across a traverse for Kwohl Butte (sample 8509053). A) An content (mol %) plotted versus distance from core to rim of sample. B) Nomarski differential interference contrast image of crystal with microprobe traverse plotted for reference. Crystal is classified as IT.

A

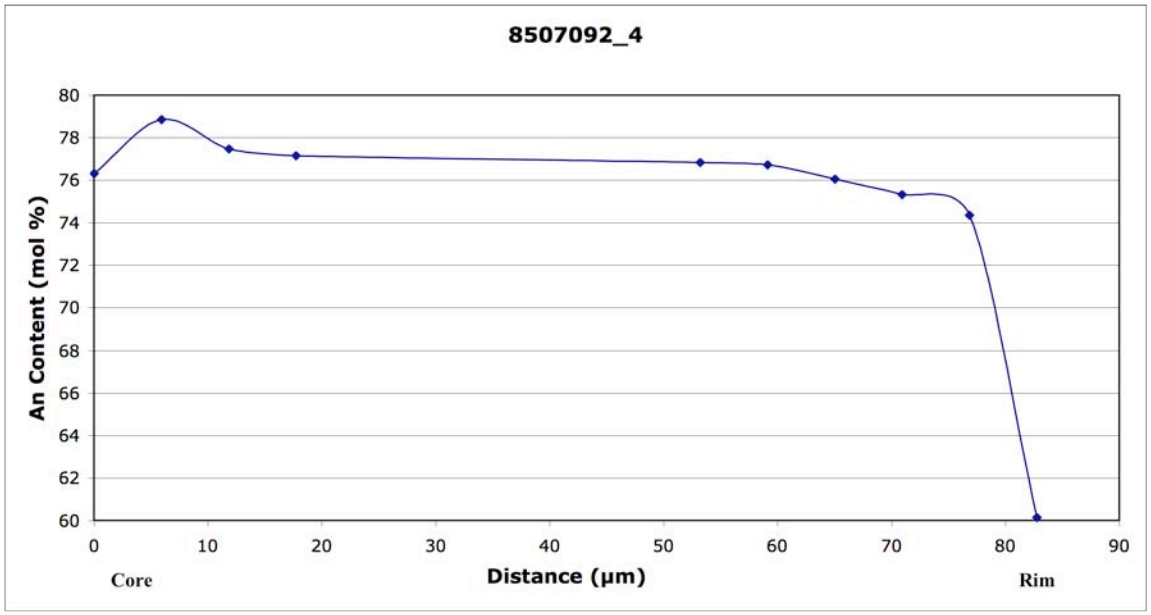

B

Figure 15. Anorthite content across a traverse for Kwohl Butte (sample 8507092). A) An content (mol %) plotted versus distance from core to rim of sample. B) Nomarski differential interference contrast image of crystal with microprobe traverse plotted for reference. Crystal is classified as IT.

example of this is sample 8407294, shown in Figure 13, which shows a decrease in anorthite within approximately 50 μm of the rim.

Microlite Analyses

The cores of seven microlites were analyzed for each of the five samples. Areas that were analyzed were chosen using electron back-scatter diffraction images acquired with the electron microprobe. Analyses that were contaminated were excluded based on the MgO, FeO, and SiO_2 values. Table 6 expresses the average An, Or, and Ab contents, as well as one standard deviation, for the analyzed microlites.

TABLE 6. AVERAGE ANORTHITE, ORTHOCLASE, AND ALBITE COMPOSITIONS FOR ANALYZED MICROLITES

Episode III unit	Sample number	An ± 1σ	Or ± 1σ	Ab ± 1σ
Tot Mountain	8407254	46.47 ± 15.1	2.79 ± 1.4	50.74 ± 13.7
Bachelor Cap	8409132	46.70 ± 3.4	2.20 ± 0.3	51.11 ± 3.1
Bachelor Shield	8407294	55.02 ± 7.0	1.79 ± 0.6	43.20 ± 6.4
Kwohl Butte	8509053	57.99 ± 0.9	1.52 ± 0.1	40.49 ± 1.0
Kwohl Butte	8507092	53.40 ± 5.6	2.39 ± 0.5	44.21 ± 5.0

Notes: An—anorthite; Or—orthoclase; Ab—albite.

Average anorthite contents for all samples fall between An_{46} to An_{58}, ranging from andesine ($An_{30–50}$) to labradorite. Graphs illustrating the anorthite content for all microlites are presented in Data File L. A comparison of average anorthite content for phenocrysts and microphenocrysts compared to microlites for each sample is expressed in Table 7. It is shown that the anorthite content in microlites is significantly lower.

ICP-MS Trace Element Data

Trace elements analyzed include La, Ce, Pr, Nd, Sm, Eu, Gd, Tb, Dy, Ho, Er, Tm, Yb, Lu, Ba, Th, Nb, Y, Hf, Ta U, Pb, Rb, Cs, Sr, Sc, and Zr. All analyses are recorded in

TABLE 7. AVERAGE ANORTHITE CONTENT FOR PHENOCRYSTS, MICROPHENOCRYSTS, AND MICROLITES

Episode III unit	Sample number	ph	mph	ml
Tot Mountain	8407254	69.76	59.94	46.47
Bachelor Cap	8409132	63.90	71.72	46.70
Bachelor Shield	8407294	72.61	72.98	55.02
Kwohl Butte	8509053	72.85	74.30	57.99
Kwohl Butte	8507092	69.66	59.09	53.40

Notes: ph—phenocrysts; mph—microphenocrysts; ml—microlites.

parts per million (ppm) and are reported in Data File A. Major element and Ni and Cr data from Gardner (1994b) and trace-element data from this study were plotted to document elemental and oxide relationships (Figure 16–18). Figure 16 illustrates the most significant oxide comparisons to MgO and Figures 17 and 18 illustrate the most significant trace element comparisons to MgO. These figures include comparisons of MgO to SiO_2, CaO, Al_2O_3, and Fe_2O_3, as well as Sr, Ni, Cr, Y, Th, Nd, Rb, and Pb. The remaining plots, including oxide and ICP-MS data compared to the relative stratigraphic position, are presented in Data Files M and N.

In general, with increasing MgO, a negative correlation is observed for oxide data SiO_2, Al_2O_3, Na_2O, and K_2O and trace element data Sr, Y, Th, Nd, Rb, Pb, Cs, La, Ce, Lu, Hf, Yb, Ba, U, Dy, Sm, Tm, Zr and Gd. A positive correlation with increasing MgO is observed for oxide data CaO, FeO,TiO_2 and MnO and trace elements Ni, Cr, Sc, Eu, and Nb. The trace element Ta demonstrated neither a positive nor a negative correlation.

Chondrite-normalized REE diagrams were constructed to compare REE of the Bachelor series to chondritic meteorites (Winter, 2001; Wilson, 1989). Figures 19–21 illustrate the REE relationships of the three main units, Bachelor Cap and Tot Mountain, Bachelor Shield, and Kwohl Butte. Figure 19 illustrates the REE for lavas from Bachelor

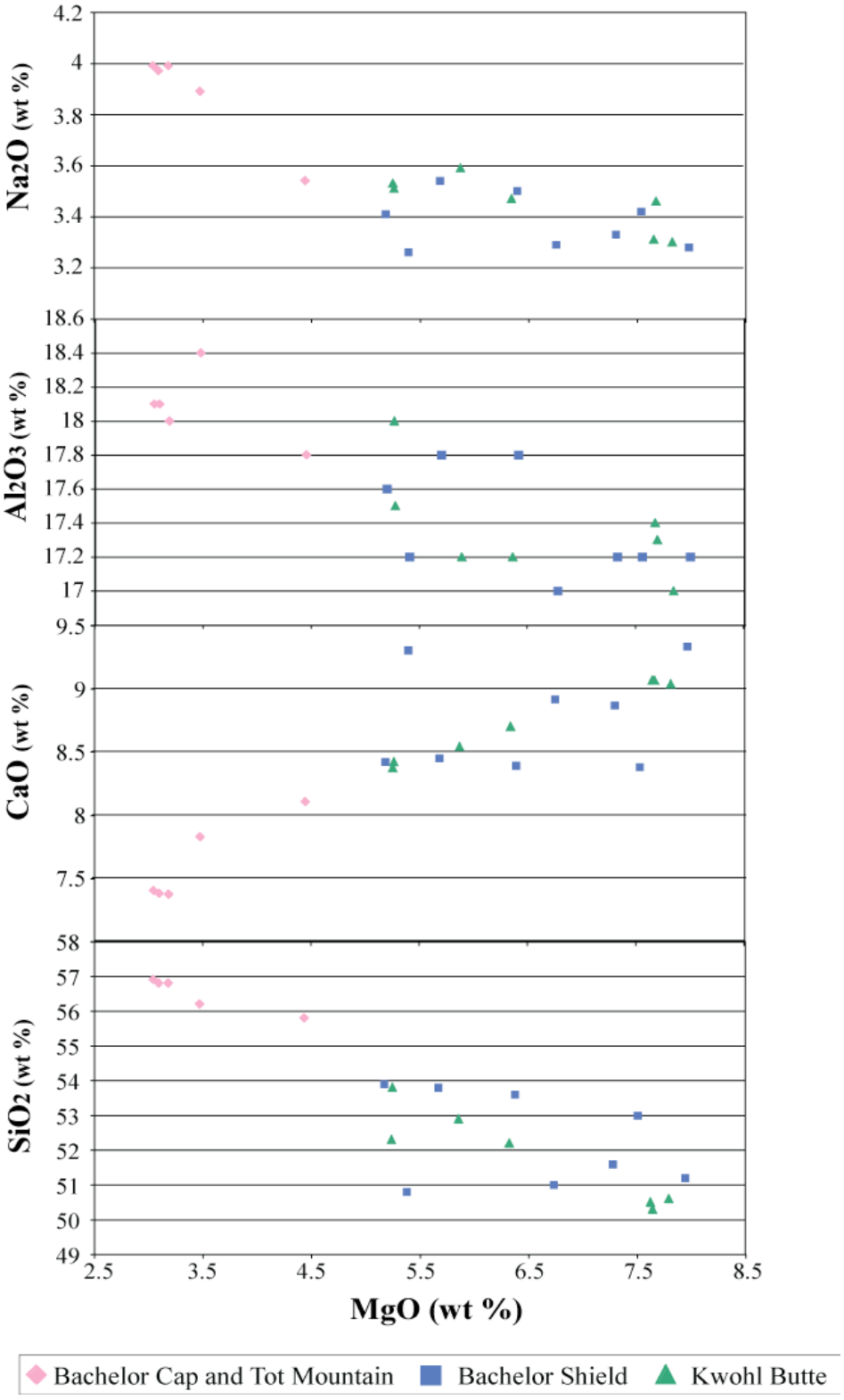

Figure 16. Binary plots of wt % MgO versus oxides SiO_2, CaO, Al_2O_3, and Na_2O.

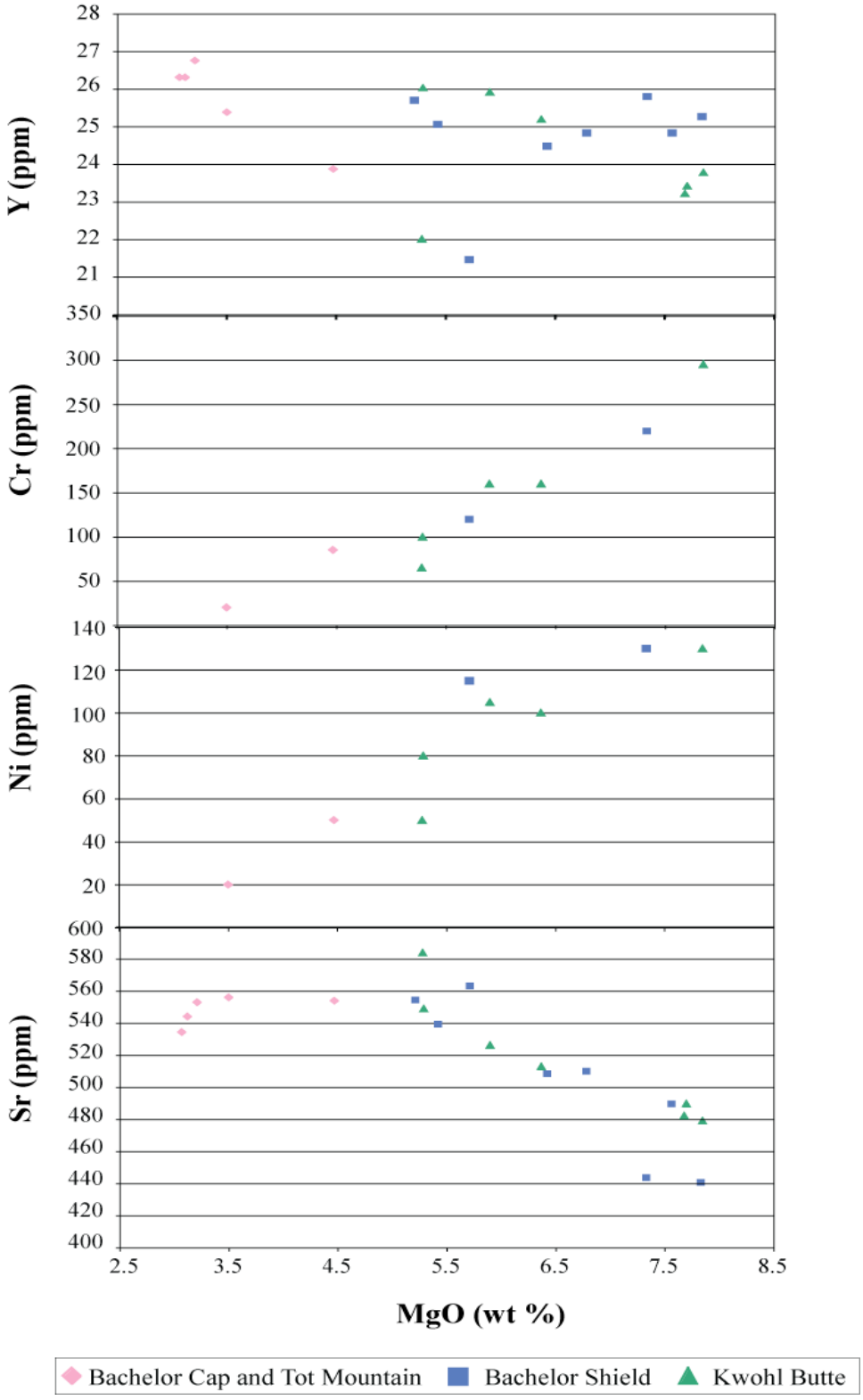

Figure 17. Binary plots of wt % MgO versus trace elements Sr, Ni, Cr, and Y.

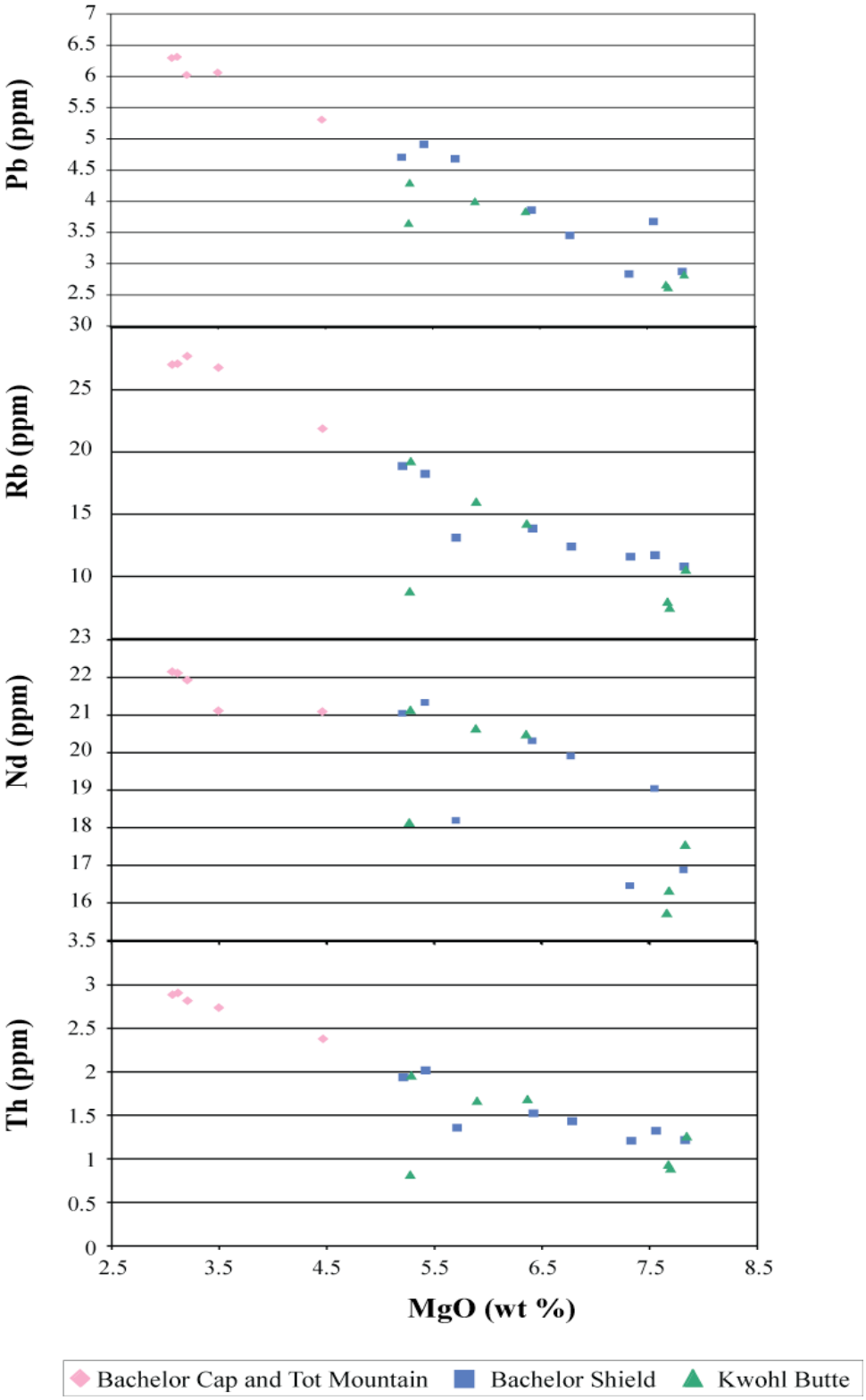

Figure 18. Binary plots of wt % MgO versus trace elements Th, Nd, Rb, and Pb.

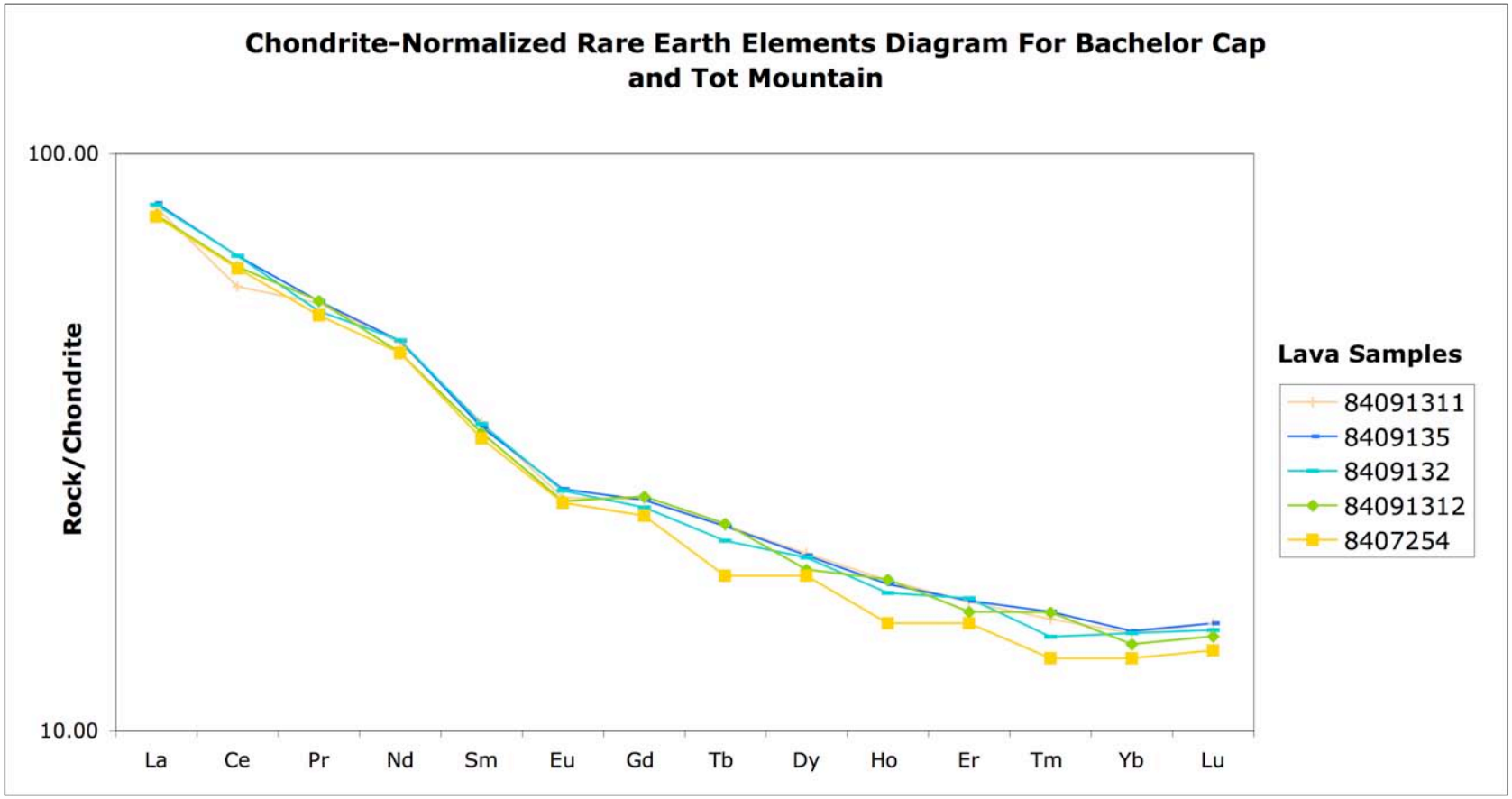

Figure 19. Chondrite-normalized REE diagram for Bachelor Cap and Tot Mountain lavas.

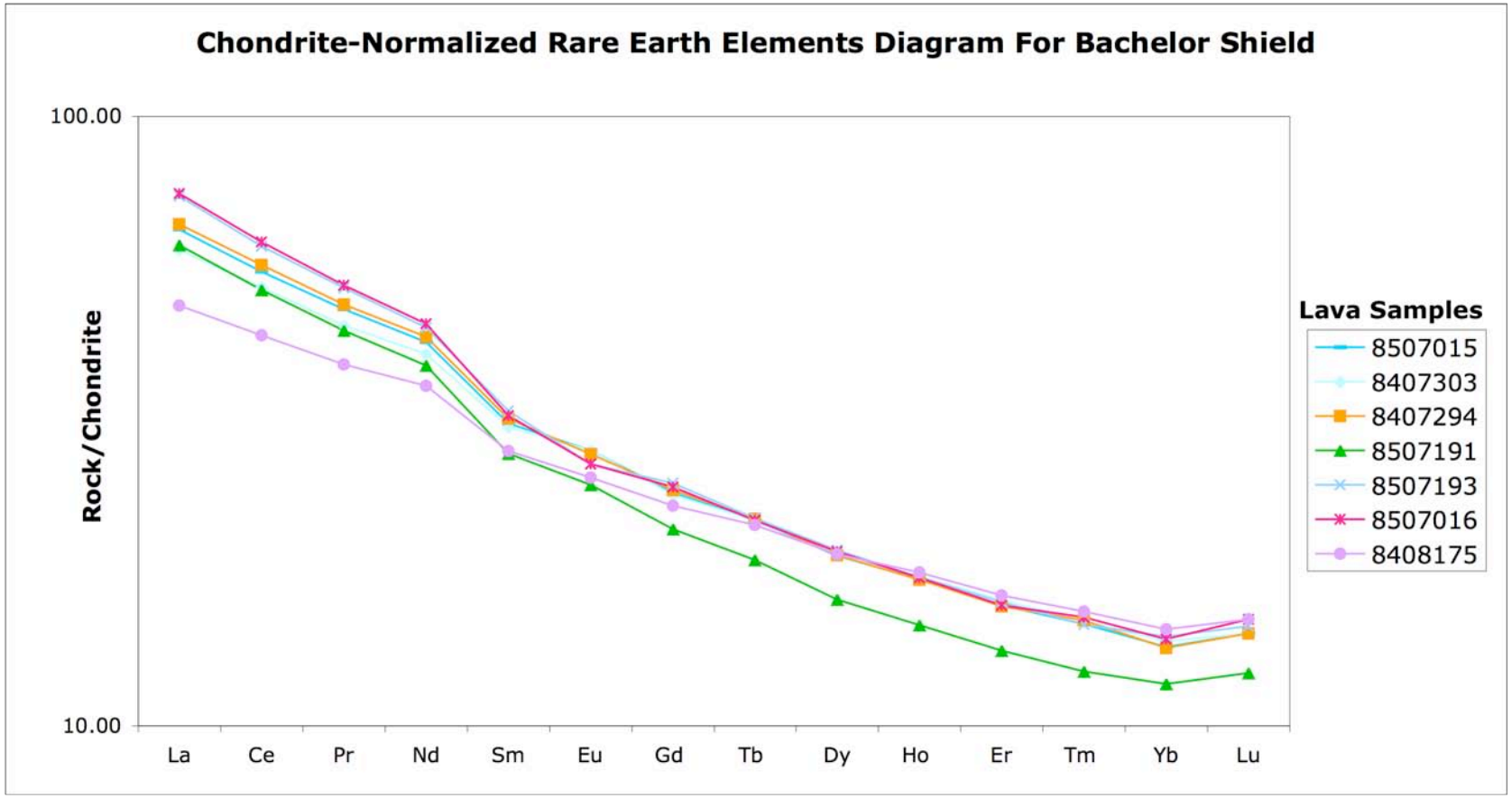

Figure 20. Chondrite-normalized REE diagram for Bachelor Shield lavas.

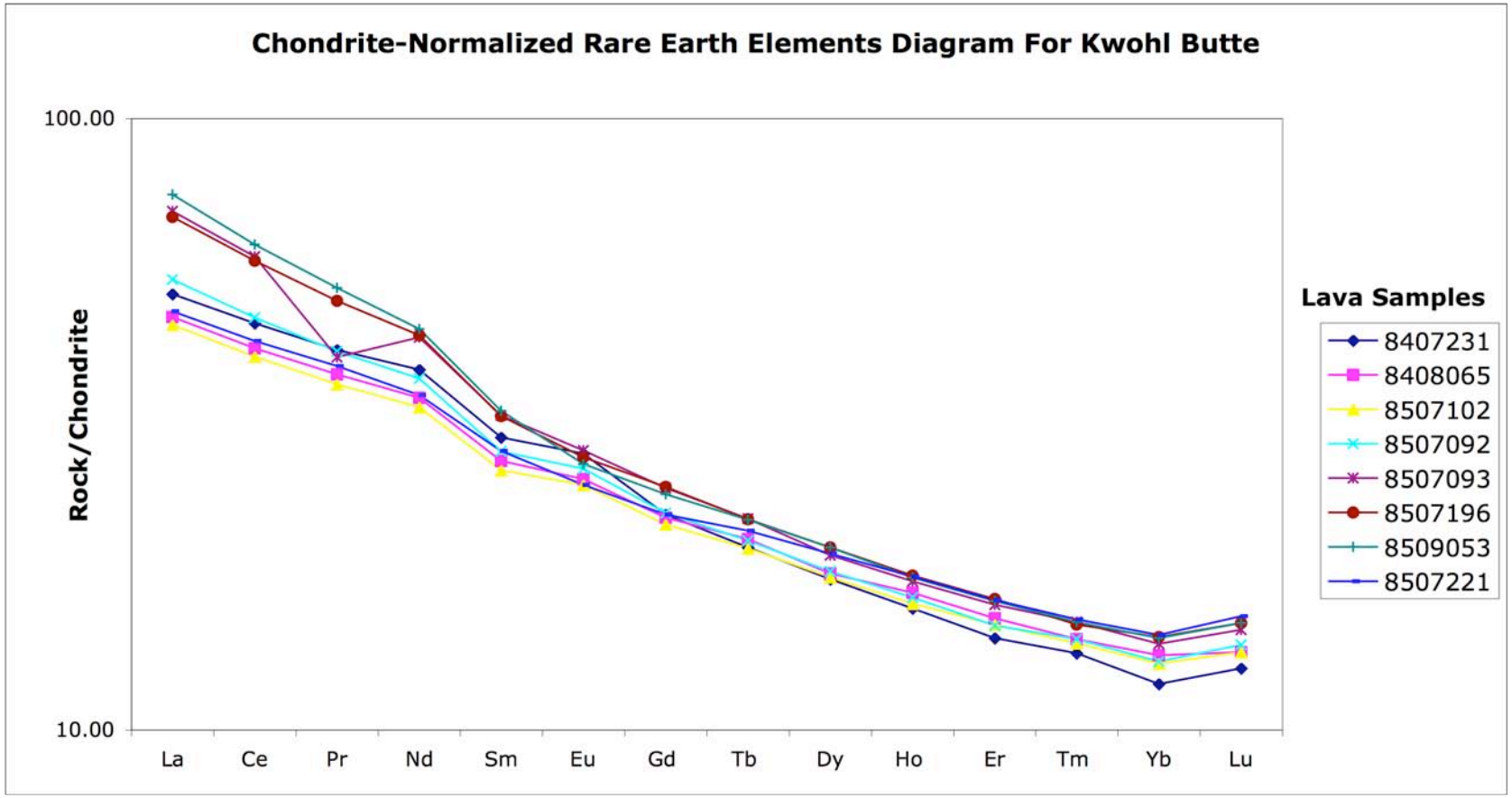

Figure 21. Chondrite-normalized REE diagram for Kwohl Butte lavas.

Cap and Tot Mountain. The expected negative trend in REE is observed with only a slight increase in Lu. Figure 20 illustrates the REE for lavas from Bachelor Shield. A positive Eu anomaly is observed for samples 8507191 and 8407294 in the REE for these lavas, as well as the increase in Lu. The remaining samples show neither a positive or negative anomaly. Figure 21 illustrates the REE for lavas from Kwohl Butte. A similar positive Eu anomaly is observed in these several lavas, as well as the increase in Lu observed in the other three units. Very little variation is observed in the REE trends of samples in the study.

Sr and Nd Isotope Ratio Data

Twenty whole-rock samples were analyzed for $^{143}Nd/^{144}Nd$ and $^{87}Sr/^{86}Sr$. Two select samples from Kwohl Butte (8507092) and Bachelor Cap (8409132) were subsequently selected from the original 20 samples for single crystal Sr isotope analysis. A range of ratios from 0.512846 to 0.512963 exists for the $^{143}Nd/^{144}Nd$ whole-rocks and from 0.703511 to 0.703788 for the $^{87}Sr/^{86}Sr$ whole-rocks. Single grain $^{87}Sr/^{86}Sr$ range from 0.703526 to 0.704890 for sample 8507092, and 0.703748 to 0.704109 for sample 8409132.

Whole-Rock $^{143}Nd/^{144}Nd$

Whole-rock Nd isotope values range from 0.512813±10 to 0.512963±12, and analytical uncertainty is no greater than 0.000015. Table 8 lists $^{143}Nd/^{144}Nd$ in stratigraphic order with the youngest unit, Tot Mountain, at the top. Figure 22 presents $^{143}Nd/^{144}Nd$ in stratigraphic order with the 2-sigma uncertainty bars. A gradual decrease in $^{143}Nd/^{144}Nd$ is observed with decreasing age. Tot Mountain and Bachelor Cap show the

TABLE 8. $^{143}Nd/^{144}Nd$ ISOTOPE RATIOS IN STRATIGRAPHIC ORDER

Sample number	$^{143}Nd/^{144}Nd$	2-sigma uncertainty
Tot Mountain		
8407254	0.512846	0.000009
Bachelor Cap		
84091312	0.512813	0.000010
8409132	0.512853	0.000010
8409135	0.512886	0.000012
84091311	0.512849	0.000010
Bachelor Shield		
8408175	0.512904	0.000008
8507016	0.512861	0.000009
8507193	0.512869	0.000009
8507191	0.512850	0.000010
8407294	0.512907	0.000008
8407303	0.512939	0.000008
8507015	0.512918	0.000009
8507221	0.512895	0.000009
Kwohl Butte		
8509053	0.512865	0.000008
8507196	0.512891	0.000007
8507093	0.512911	0.000008
8507092	0.512947	0.000015
8507102	0.512935	0.000009
8408065	0.512963	0.000012
8407231	0.512897	0.000010

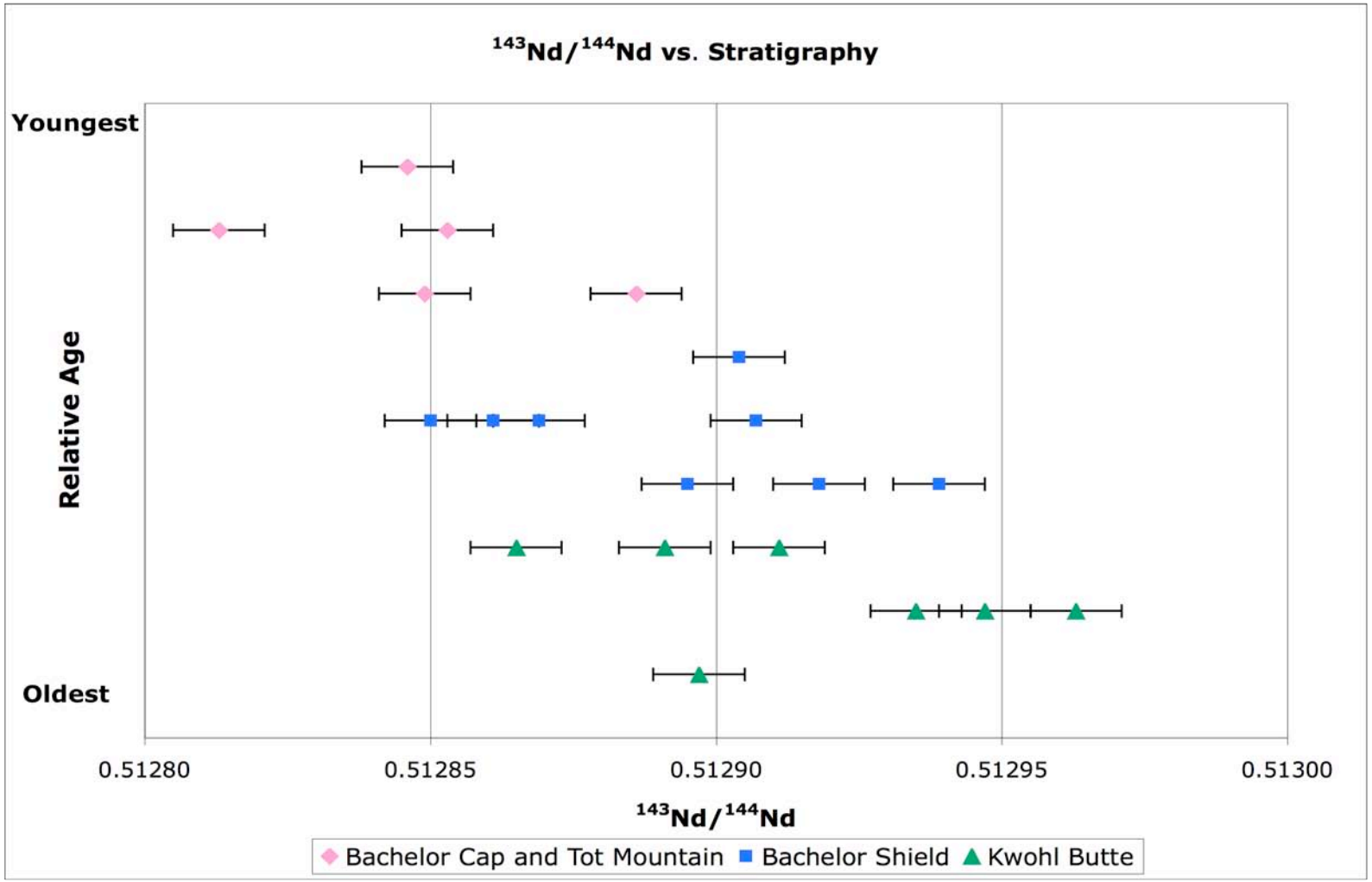

Figure 22. Binary plot of whole-rock $^{143}Nd/^{144}Nd$ versus relative stratigraphic order.

lowest isotopic ratios, whereas Kwohl Butte and Bachelor Shield have the highest. Within specific units, isotopic variability also exists. Kwohl Butte $^{143}Nd/^{144}Nd$ range from 0.512865 to 0.512963. Bachelor Shield $^{143}Nd/^{144}Nd$ range from 0.512850 to 0.512939. Finally, Bachelor Cap $^{143}Nd/^{144}Nd$ range from 0.512813 to 0.512886. Tot Mountain falls with the Bachelor Cap $^{143}Nd/^{144}Nd$ range.

Whole-Rock $^{87}Sr/^{86}Sr$

Whole-rock Sr isotope analyses range from 0.703425 to 0.703788 and analytical uncertainty is no greater than 0.000020. Table 9 lists all $^{87}Sr/^{86}Sr$ isotopic ratios in stratigraphic order with the youngest unit, Tot Mountain, at the top. Figure 23 presents $^{87}Sr/^{86}Sr$ in stratigraphic order with the associated 2-sigma bars. Kwohl Butte and Bachelor Shield show more isotopic variability than Bachelor Cap and Tot Mountain. Isotopic ratios range from 0.703439 to 0.703759 at Kwohl Butte and from 0.703425 to 0.703690 at Bachelor Shield. Bachelor Cap and Tot Mountain show little isotopic variation, all falling within 0.000026 of each other.

Single Crystal Sr Isotope Ratio Data

Single crystals obtained from two samples from this study were analyzed for $^{87}Sr/^{87}Sr$ values. Sample 8507092 is from Kwohl Butte and sample 8409132 is from Bachelor Cap. Plagioclase grains for both samples were collected based on visual inspection. Priority was given to those crystals lacking visible melt inclusions, because melt may have significantly different $^{87}Sr/^{87}Sr$ than crystals. In addition, four olivine grains from 8409132 and two samples of an unknown white material (WM) from 8507092 were also collected for isotope analysis. Tables 10 and 11 summarize sample

TABLE 9. $^{87}Sr/^{86}Sr$ ISOTOPE RATIOS IN STRATIGRAPHIC ORDER

Sample Number	$^{87}Sr/^{86}Sr$	2-sigma uncertainty
Tot Mountain		
8407254	0.703788	0.000014
Bachelor Cap		
84091312	0.703781	0.000010
8409132	0.703774	0.000011
8409135	0.703764	0.000008
84091311	0.703762	0.000011
Bachelor Shield		
8408175	0.703511	0.000008
8507016	0.703690	0.000010
8507193	0.703690	0.000008
8507191	0.703612	0.000010
8407294	0.703524	0.000008
8407303	0.703425	0.000015
8507015	0.703525	0.000008
8507221	0.703536	0.000008
Kwohl Butte		
8509053	0.703679	0.000008
8507196	0.703759	0.000007
8507093	0.703536	0.000008
8507092	0.703679	0.000008
8507102	0.703506	0.000020
8408065	0.703439	0.000010
8407231	0.703743	0.000008

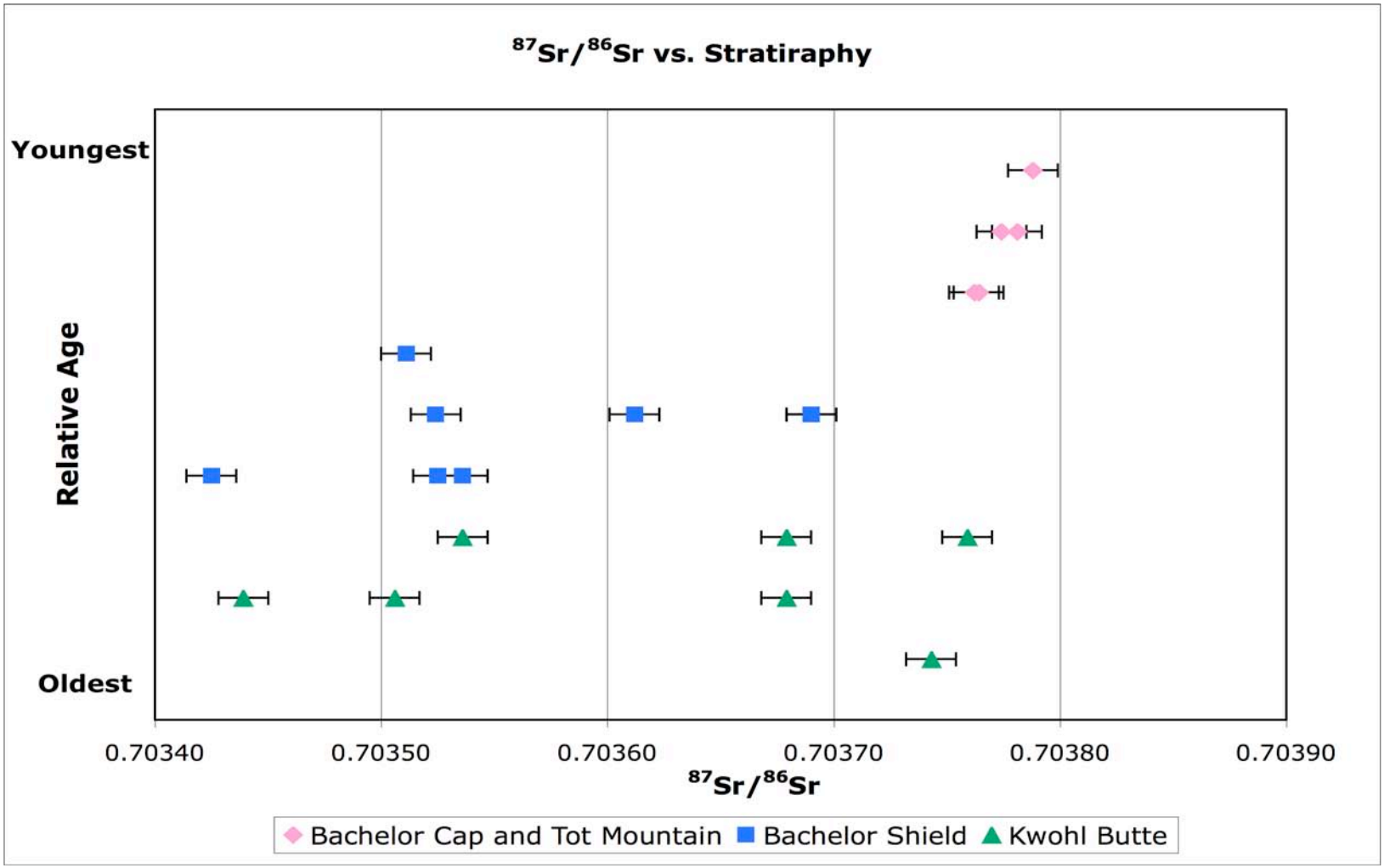

Figure 23. Binary plot of whole-rock $^{87}Sr/^{86}Sr$ versus relative stratigraphic order.

TABLE 10. SINGLE CRYSTAL $^{87}Sr/^{86}Sr$ ISOTOPIC RATIOS FROM SAMPLE 8409132 (BACHELOR CAP)

Sample number	Sample type	Mass (mg)	Sr mass (ng)†	Spike addition (g)	$^{87}Sr/^{86}Sr$	2-sigma uncertainty
8409132-A	Plagioclase	0.749	646	N/A	0.704109	0.000008
8409132-B	Plagioclase	0.910	784	N/A	0.703794	0.000014
8409132-C	Plagioclase	0.051	44	N/A	0.703870	0.000050
8409132-D	Olivine (4 Grains)	0.664	0.005‡	N/A	0.703810	0.000050
8409132-E	Plagioclase	0.082	71	N/A	0.703779	0.000010
8409132-F	Plagioclase	0.127	109	N/A	0.703748	0.000049
8409132-G	Plagioclase	0.086	74	N/A	0.703747	0.000008
8409132-H	Plagioclase	0.094	81	N/A	0.703762	0.000010
8409132-I	Plagioclase	0.71	61	N/A	0.703779	0.000011
8409132-J	Plagioclase	0.63	54	N/A	0.703758	0.000010
8409132-K	Plagioclase	0.84	72	N/A	0.703790	0.000010
8409132-L	Plagioclase	0.170	147	N/A	0.703786	0.000008
8409132-M	Plagioclase	0.145	337§	0.1378	0.704878	0.000010

† Calculated Sr mass for sample 8409132: Mineral Sr concentration (743 ppm) was calculated from the spiked sample 8507092-B and divided by the whole-rock Sr concentration from sample 85070923 (479 ppm) from inductively coupled plasma mass spectrometry (ICP-MS) analysis (this study) to determine the mineral melt partition coefficient, D_{Sr} (1.55). D_{Sr} (1.55) was multiplied by the whole-rock concentration for sample 8409132 (556 ppm) to determine the mineral Sr concentrations (862 ppm) (mineral Sr concentration). The mineral Sr concentration was then multiplied by the mass of the sample to determine Sr mass for each crystal.

‡ Calculated Sr mass for sample 8409132 olivine crystals: The mineral melt coefficient, 0.014, from Rollinson (1983) was multiplied by the whole-rock concentration (479 ppm) obtained from ICP-MS (this study) to determine the mineral Sr concentration (7 ppm). The mineral Sr concentration was then multiplied by the mass of the sample to determine Sr mass for the olivine crystals.

§ Sample 8409132-M: Mineral Sr concentration (2,320 ppm) was calculated for the spiked sample 8409132-M, resulting in a mineral melt partition coefficient of 4.17. Sr concentration and $^{87}Sr/^{86}Sr$ are atypical from other crystals from sample 8409132. See text for interpretations.

TABLE 11. SINGLE CRYSTAL $^{87}Sr/^{86}Sr$ ISOTOPIC RATIOS FROM SAMPLE 8507092 (KWOHL BUTTE)

Sample number	Sample type	Mass (mg)	Sr mass (ng)†	Spike addition (g)	$^{87}Sr/^{86}Sr$	2-sigma uncertainty
8507092-A	Plagioclase	0.336	250	N/A	0.703562	0.000011
8507092-B	Plagioclase	0.196	146	0.149	0.703748	0.000011
8507092-D	Plagioclase	0.117	87	N/A	0.703575	0.000017
8507092-E	Plagioclase	0.597	444	N/A	0.703526	0.000008
8507092-F	Plagioclase	0.136	101	N/A	0.703546	0.000056
8507092-G	Plagioclase	0.073	54	N/A	0.703546	0.000011
8507092-J	WM-2	0.797	N/A	N/A	0.704890	0.000033
8507092-O	WM-3	1.879	N/A	N/A	0.703418	0.000008

† Calculated Sr mass for sample 8507092: Mineral Sr concentration (743 ppm) was calculated from the spiked sample 8507092-B. The mineral Sr concentration was then multiplied by the mass of the sample to determine Sr mass for each crystal.

type (plagioclase single crystal, crystal aggregates of olivine), sample mass, the mass of Sr in each sample, the mass of Sr spike, the final $^{87}Sr/^{86}Sr$, and the associated 2-sigma uncertainty.

Isotopic ratios from the single grains were compared to the whole-rock $^{87}Sr/^{86}Sr$ mentioned above. Single crystal $^{87}Sr/^{86}Sr$ for sample 8409132 range from 0.703747 ± 8 to 0.704878 ± 10 and the whole-rock isotope ratio for this sample is 0.703774 ± 11 (Figure 24). Most of the crystals are within or close to within analytical uncertainty of the whole-rock value. There are three plagioclase crystals that are exceptions. These crystals (8409132-A, 8409132-C, and 8409132-M) are more radiogenic than the other crystals and the whole-rock value.

Single crystal $^{87}Sr/^{86}Sr$ for sample 8507092 range from 0.703418 ± 8 to 0.704890 ± 33 (Figure 25) and the $^{87}Sr/^{86}Sr$ isotope ratios for the single crystals typically fall within 0.000010 of each other. The whole-rock isotope ratio for this sample is 0.703679 ± 8.

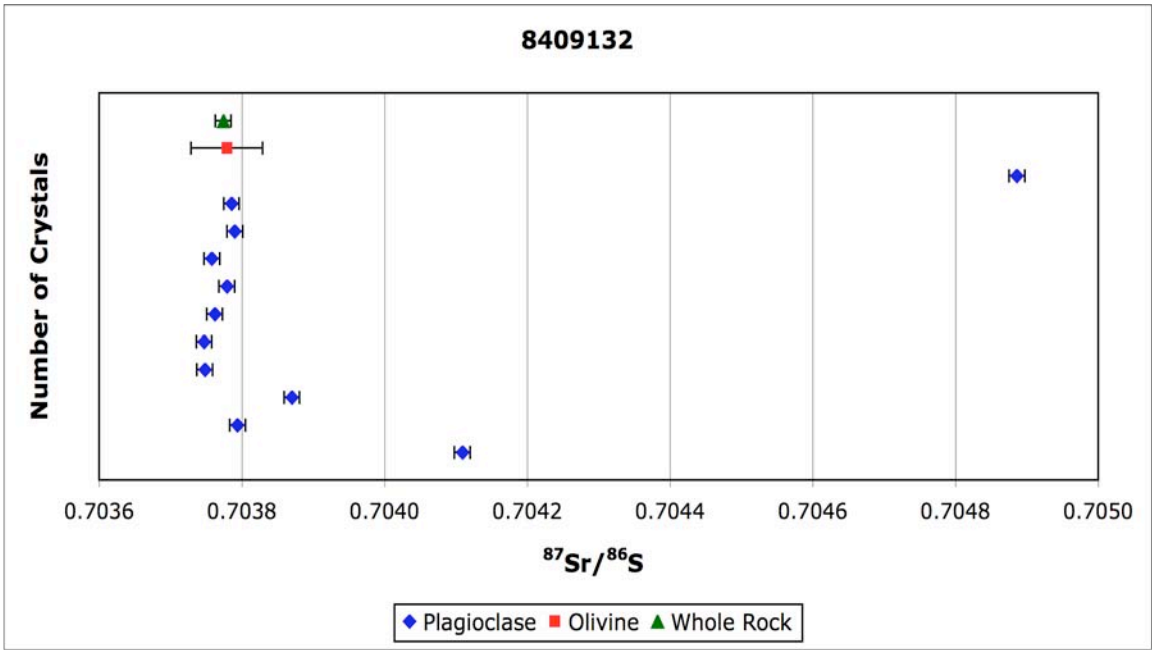

Figure 24. $^{87}Sr/^{86}Sr$ for single crystals and whole-rock from sample 8409132 (Bachelor Cap). Includes data for plagioclase, olivine, and whole-rock.

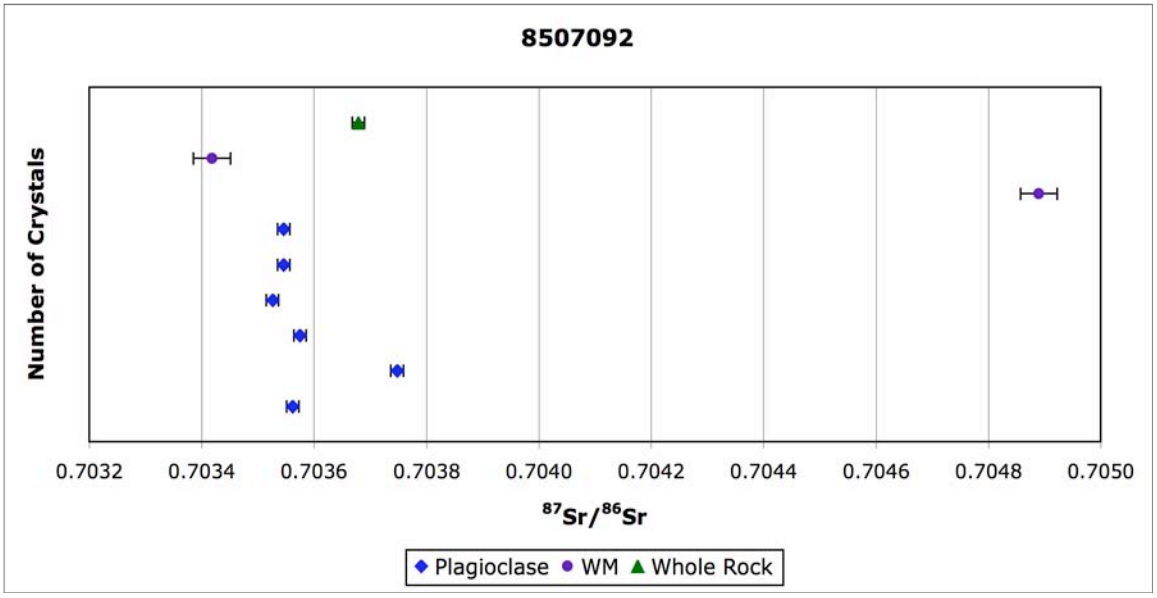

Figure 25. $^{87}Sr/^{86}Sr$ for single crystals and whole-rock from sample 8507092 (Kwohl Butte). Includes data for plagioclase crystals, white material (WM), and whole-rock.

Most crystals are not within analytical uncertainty of the whole-rock isotope value. The one exception is 8507092-B, which has a value higher than the whole-rock and the other plagioclase crystals. The unknown white material is also not in equilibrium with the whole-rock value. These samples, 8507092-J and 8507092-M, have $^{87}Sr/^{86}Sr$ of 0.704890 ± 33 and 0.703418 ± 8. Sample 8507092-J (0.704890 ± 33) is significantly higher than the whole-rock isotope value, whereas sample 8507092-M (0.703418 ± 8) is lower than the whole-rock isotope value.

CHAPTER V

DISCUSSION

Magmatic Processes Elucidated Through Analysis of Whole-Rock Data

In order to examine the relative roles of different magmatic processes, the whole-rock data were evaluated. This allows for the assessment of any effects caused by open- or closed-system processes that may have affected the magmas prior to eruption. Relevant whole-rock data includes oxides, major, and trace elements and Sr and Nd isotopes. These analyses provide some insight into the roles of crystal fractionation, assimilation, and possible recharge that has influenced the lavas of episode III at the MBVC.

Evidence for Crystal Fractionation from Major and Trace Element Data

Basalt and basaltic andesite lavas from episode III have SiO_2 values between 50 to 57 wt % and MgO values between 3 and 8 wt %. Increases in SiO_2, Al_2O_3, and Na_2O with decreasing MgO are observed from the older units (Kwohl Butte and Bachelor Shield) to the younger units (Bachelor Cap and Tot Mountain), whereas CaO decreases with decreasing MgO from the older units to the younger units. Correlations between major and trace elements are summarized in Table 12. These trends provide evidence for geochemical changes from Kwohl Butte to the Bachelor Cap and Tot Mountain units that are most consistent with the process of crystal fractionation (Figure 16). Decreasing MgO with increasing SiO_2 is indicative of the removal of MgO in the form of olivine by crystal fractionation. Because Ca is a common component of both anorthitic plagioclase feldspar and clinopyroxene, decreasing CaO with decreasing MgO may suggest

TABLE 12. SUMMARY OF GEOCHEMICAL TRENDS

Mineral phase	Magmatic process	Major element evidence	Trace element evidence	Correlation with decreasing MgO
Plagioclase	Accumulation	Al_2O_3, Na_2O	Sr	Al_2O_3, Sr: negative correlation
Clinopyroxene	Fractionation	CaO	Cr, Y	CaO, Cr, Y: positive correlation
Olivine	Fractionation	MgO	Ni	Ni: positive Correlation
Apatite	Fractionation	P_2O_5	N/A	P_2O_5: positive correlation
Fe-Ti Oxides	Fractionation	Fe-Ti oxides	N/A	Fe and Ti: positive correlation

fractionation of these mineral phases. Fractionation of plagioclase feldspar would generally cause a decrease in Al_2O_3 with decreasing MgO; therefore, it is necessary to assess Al_2O_3 to determine the crystal phase that formed. Al_2O_3 is a dominant oxide in plagioclase feldspar and is present in clinopyroxene, but in smaller abundances. The positive MgO versus Al_2O_3 trend suggests that plagioclase feldspar is not being fractionated. The positive Na_2O versus MgO trend is consistent with fractionation of olivine and clinopyroxene. It is apparent, however, from petrographic analysis that plagioclase feldspar is a dominant crystal phase. The presence of plagioclase feldspar, combined with the Al_2O_3 versus MgO trend, suggests that there was inefficient plagioclase separation during magma evolution.

Additional oxide versus MgO plots are presented in Data File M and provided evidence for the separation of clinopyroxene and olivine and the apparent lack of separation of plagioclase feldspar. Slight decreases in Fe and Ti with decreasing MgO suggest fractionation of Fe-Ti oxides. Fe can be compatible in olivine and Ti can be compatible in clinopyroxene, thus possibly causing the observed positive trends. K_2O

increases with decreasing MgO, consistent with fractionation of olivine and clinopyroxene. Apatite separation is suggested by the slight decrease in P_2O_5 with decreasing MgO, although this phase seems to be only an accessory mineral and is observed only in Bachelor Cap and Tot Mountain thin sections. The oxide data indicate the crystal separation of clinopyroxene and olivine as dominant crystal phases, with Fe-Ti oxides, and potentially apatite as accessory minerals. The data suggest plagioclase was stable but did not separate.

Analyses obtained from ICP-MS illustrated in Figures 17 and 18 include Sr, Ni, Cr, Y (Figure 17), Th, Nd, Rb, and Pb (Figure 18). These trace elements can be assessed to determine the mineral phases involved in crystal fractionation. Sr is typically used as a proxy for anorthitic plagioclase feldspar, as the Sr substitutes for Ca in the crystal lattice. Sr, however, is incompatible in clinopyroxene. Sr increases with decreasing MgO, corresponding to the lack of plagioclase feldspar separation. Cr and Y are typically used as a proxy for the mineral clinopyroxene. Cr and Y decrease with decreasing MgO. These trends can be attributed to the fractionation of clinopyroxene. The trace element Ni can be used as a proxy for olivine. The graph of Ni versus MgO is a positive trend, indicating that olivine is a significant fractionation phase.

The remaining elements, including Nd, Th, Rb, and Pb, are all trace elements that are considered incompatible in basalt and basaltic-andesite (Wilson, 1989; Winter, 2001). If the previous conclusions are correct and the lavas of this suite were dominated by the separation of clinopyroxene and olivine, and plagioclase feldspar did not fractionate, an expected positive trend should be observed in the trace elements. Figure 18 illustrates

positive MgO versus trace element trends for all of these elements, supporting the suggestion that none of these elements were compatible in the magmas erupted during episode III.

To better constrain the relationship of the incompatible elements, specifically the REE, chondrite-normalized REE diagrams were constructed. The diagrams for all four units show compatibility with average ocean island basalt (OIB) magmas, in which light REE are enriched and heavy REE are depleted (Wilson, 1989; Winter, 2001). It is interesting to note the Eu pattern observed in Figures 20 and 21. Eu is compatible with plagioclase feldspar. A negative anomaly is interpreted as the removal of plagioclase, whereas a positive anomaly is interpreted as accumulation of plagioclase. Some lavas from Bachelor Shield and Kwohl Butte illustrate a slight positive Eu anomaly. This is suggestive of the possible effect of plagioclase accumulation.

Assimilation and Crystal Fractionation Evidence from Sr and Nd Isotope Ratios

As discussed previously, isotope ratios for both Sr and Nd demonstrate a range in values. The heterogeneity in isotopic ratios provides an indication of open-system processes affecting the evolution of the magmas. Assimilation is typically recorded by an increase in $^{87}Sr/^{86}Sr$ and a decrease in $^{143}Nd/^{144}Nd$, whereas magma recharge is recorded by the converse: a decrease in $^{87}Sr/^{86}Sr$ and an increase in $^{143}Nd/^{144}Nd$. As observed in the plots of $^{87}Sr/^{86}Sr$ and $^{143}Nd/^{144}Nd$ against stratigraphic relationships (Figures 22 and 23), a general decrease in $^{143}Nd/^{144}Nd$ and a general increase in $^{87}Sr/^{86}Sr$ from Kwohl Butte to Bachelor Cap is observed. These trends suggest that assimilation occurred from

the oldest unit (Kwohl Butte) to the youngest units (Bachelor Cap and Tot Mountain) (Table 13). It was demonstrated the crystal fractionation of clinopyroxene and olivine is

TABLE 13. SUMMARY OF MAXIMUM AND MINIMUM ISOTOPE VALUES FOR $^{87}Sr/^{86}Sr$ AND $^{143}Nd/^{144}Nd$

Lava unit	Minimum $^{87}Sr/^{86}Sr$	Maximum $^{87}Sr/^{86}Sr$	Minimum $^{143}Nd/^{144}Nd$	Maximum $^{143}Nd/^{144}Nd$
Tot Mountain	0.703788	N/A	0.512846	N/A
Bachelor Cap	0.703762	0.703781	0.512813	0.512886
Bachelor Shield	0.703425	0.703690	0.512850	0.512939
Kwohl Butte	0.703439	0.703759	0.512865	0.512963

also a significant factor in the evolution of the erupted lavas. Crystal fractionation in a magmatic system typically results in the release of latent heat, thus providing the energy for melting of surrounding crustal material (Bowen, 1928). The large-scale isotopic trends observed in episode III rocks are consistent with the process of AFC affecting the magma systems.

Isotopic variability exists within the Kwohl Butte and Bachelor Shield units, whereas $^{87}Sr/^{86}Sr$ for Bachelor Cap and Tot Mountain are within reproducibility. Bachelor Cap and Tot Mountain are characterized by high $^{143}Nd/^{144}Nd$, although variability does exist. Both Kwohl Butte and Bachelor Shield are characterized by low $^{87}Sr/^{86}Sr$ and high $^{143}Nd/^{144}Nd$; however, there is an increase in $^{87}Sr/^{86}Sr$ and a decrease in $^{143}Nd/^{144}Nd$ up section. These trends indicate a potential recharge event among the first sample(s), followed by latent heat assimilation. There exists a bi-modal relationship between the basalts and the basaltic-andesites for both of these units. The basalts typically have lower $^{87}Sr/^{86}Sr$ ratios whereas the basaltic-andesites have higher $^{87}Sr/^{86}Sr$ ratios. Bachelor Cap and Tot Mountain generally increase up section in $^{87}Sr/^{86}Sr$,

although all values are within analytical uncertainty. The $^{143}Nd/^{144}Nd$ is more variable up section; however, the youngest unit, Tot Mountain, falls within the range of the Bachelor Cap, indicating that these two units are closely related. A Sr-Nd overlap exists between the Kwohl Butte and Bachelor Shield units, and between the Bachelor Cap and Tot Mountain units. These distinctions, although subtle, may suggest that the magma reservoirs for the Kwohl Butte–Bachelor Shield and Bachelor Cap–Tot Mountain units are physically distinct.

A comparison of $^{87}Sr/^{86}Sr$ and $^{143}Nd/^{144}Nd$ is illustrated in Figure 26 with the fields for mid-ocean ridge basalts (MORB), OIB, continental crust material, and oceanic sediments (Winter, 2001). The lavas of the MBVC are situated within the OIB field. Further comparisons of the $^{87}Sr/^{86}Sr$ against $^{143}Nd/^{144}Nd$ isotopic ratios are illustrated in Figures 27–29. Figures 27 and 28 illustrate isotopic variability against MgO. Both plots depict the evolution of the isotopes with decreasing MgO. The data illustrate a separation between the lavas of the Bachelor Shield and Kwohl Butte from Bachelor Cap and Tot Mountain. These trends are in accordance with the suggestions that assimilation is important and there may be physical separation between magma systems for these units. Figure 29 illustrates the relationship between $^{143}Nd/^{144}Nd$ and Nd concentrations. There is evidence of isotopic evolution with increasing elemental concentration. It is apparent that the lavas of Bachelor Cap and Tot Mountain show less variability in elemental abundances.

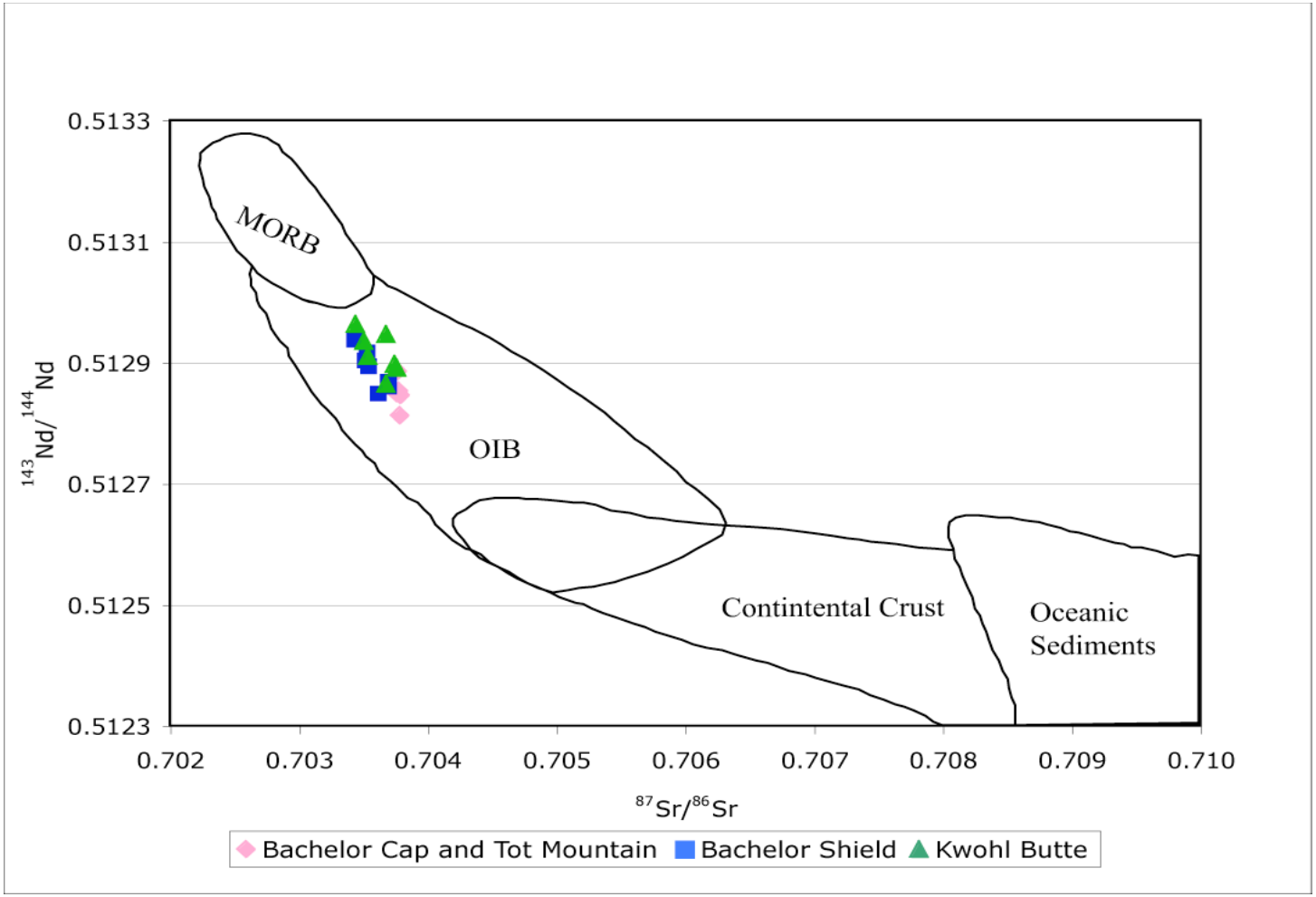

Figure 26. $^{87}Sr/^{86}Sr$ versus $^{143}Nd/^{144}Nd$. Fields include MORB, OIB, continental crust, and oceanic sediment values (Winter, 2001). Data from the MBVC plot within the OIB field.

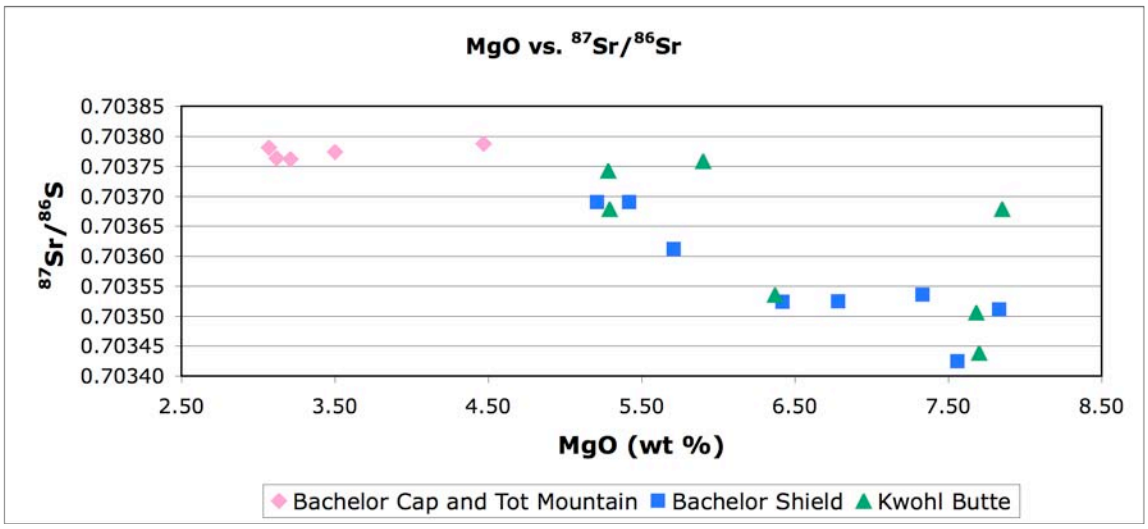

Figure 27. Binary plot of MgO versus $^{87}Sr/^{86}Sr$.

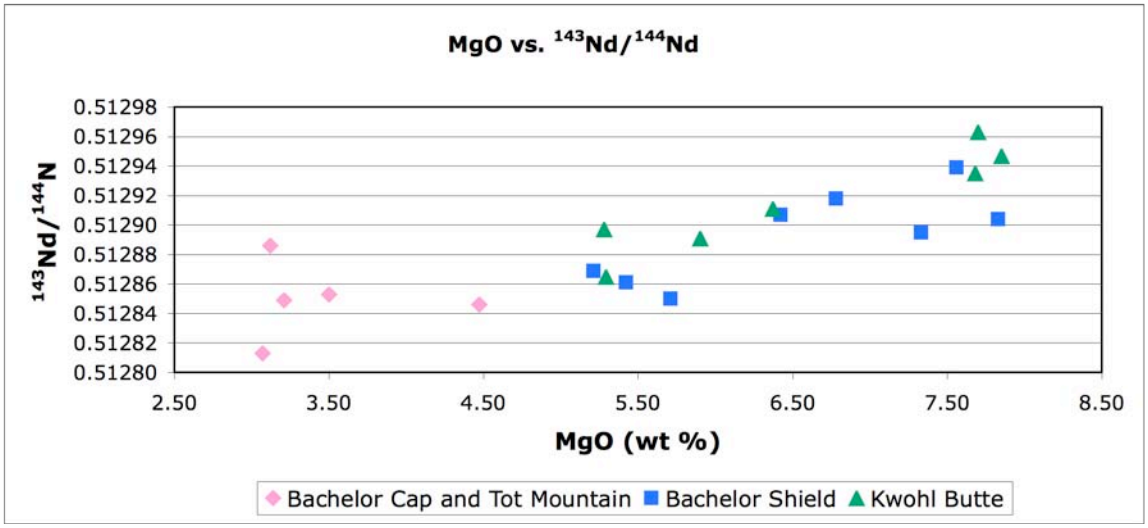

Figure 28. Binary plot of MgO versus $^{143}Nd/^{144}Nd$.

Magmatic Processes Elucidated Through Analysis of Single Crystal Data

To further constrain the magmatic processes affecting the lavas of episode III, focus was placed on five samples that are representative of episode III compositions and stratigraphy. By analyzing individual crystals, geochemical signatures can be

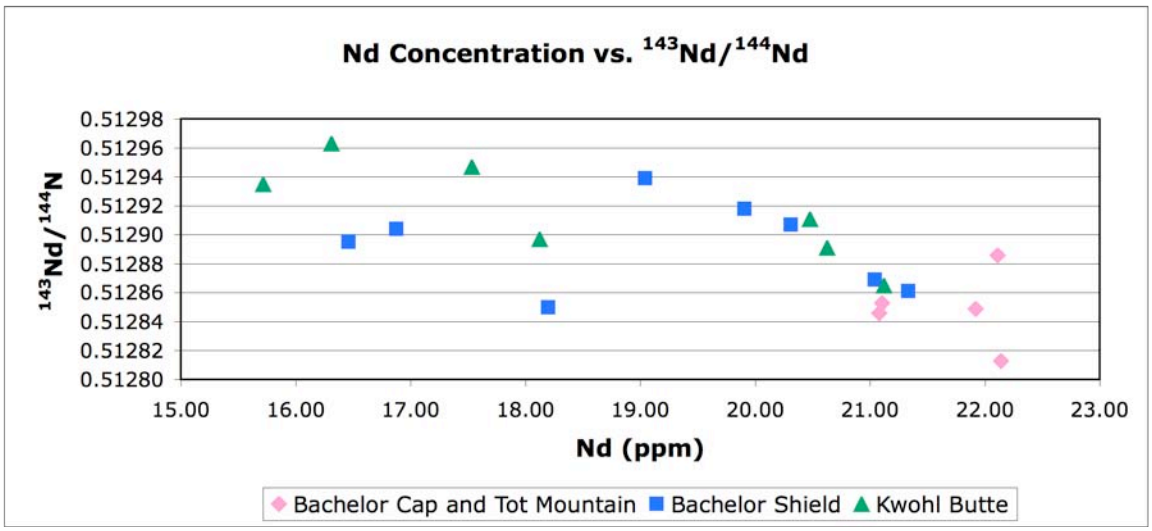

Figure 29. Binary plot of Nd concentration versus $^{143}Nd/^{144}Nd$.

documented that would otherwise be masked by the whole-rock component (Turner et al., 2003; Davidson et al., 2005). Analysis of plagioclase feldspar is important because as crystals grow, concentric zones develop. These zones act as recorders of the geochemical conditions in which the crystal grew (Anderson, 1983; Pearce and Kolisnik, 1990; Kohut and Nielson, 2003). Plagioclase feldspar isotope analyses provide information about the isotopic characteristics of an evolving magma system as the crystal grows (Fleck, 1990; Singer et al., 1995; Ramos and Reid, 2005; Lundstrom and Tepley, 2006). By focusing on single crystal plagioclase feldspar, interpretation of the isotopic conditions in which the crystal grew can be better assessed.

Electron Microprobe Geochemistry

Textural observations of the NDIC images referred to in Figures 8–10 and Data Files B–D allow plagioclase crystals to be divided into three textural types: ST, IT, and CT. All textures are observed in all units of episode III, indicating that no texture is unique to a specific unit. The majority of crystals imaged by NDIC techniques have

simple textures that provide little evidence of open-system processes having influenced this magmatic system. For example, very few resorbed crystals are observed. The lack of resorption textures, a strong indicator for potential open-system magmatic processes, suggests that perhaps the magmatic system that produced these lavas was a relatively simple system that was only slightly affected by outside processes. In contrast, the most common texture observed in intermediate and complex crystal textures is sieving.

Plagioclase feldspar from the 5 samples analyzed by electron microprobe have An contents that range from An_{61} to An_{76} for phenocrysts, An_{59} to An_{75} for microphenocrysts, and An_{46} to An_{58} for microlites. For most crystals analyzed, cores have higher An contents than rims. These trends are observed in the core and rim data described in Data File J. The core and rim anorthite content is plotted versus MgO (Figure 30). The samples from Bachelor Shield show the least variation from core to rim. The An content of plagioclase in the lavas from Tot Mountain, Bachelor Cap and Kwohl Butte illustrate a decrease in anorthite content from core to rim. Figure 30 shows a higher anorthite content for the older units, whereas the younger units have a more variable anorthite content. This is better exemplified by the rim anorthite contents. The anorthite trends for the rims suggest that Ca in the magma chamber is fractionating. This trend is also shown by the relationship of An content versus MgO. Kwohl Butte and Bachelor Shield have higher An contents, whereas Bachelor Cap and Tot Mountain have lower An content compared to MgO.

Core to rim traverses also generally show higher An content in the core and lower in the rim, with An contents ranging from An_{59} to An_{79} for all analyzed samples.

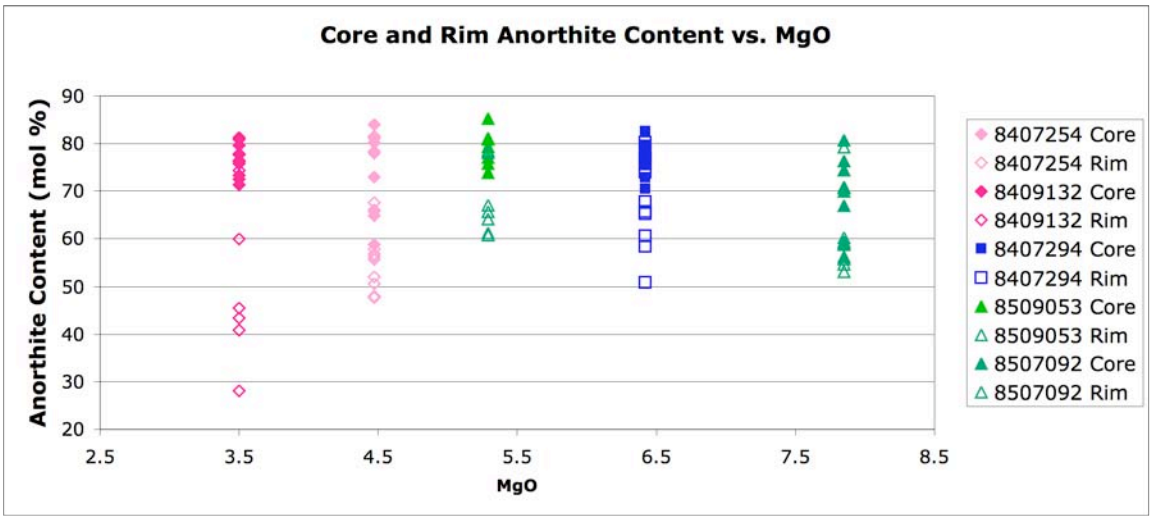

Figure 30. Binary plot of plagioclase core and rim anorthite content versus whole-rock MgO values.

Traverses also illustrate possible magmatic processes that may have affected crystals as they grew. For instance, all analyses illustrated in Figures 11–15 record regions of the crystals that grew in magmatic conditions with lower anorthite content. The variation in An contents for these crystals could be indicative of magmatic convection, which resulted in migration of crystals to areas of less mafic magma. Because magmatic systems are not necessarily compositionally homogenous, convection of the magma would result in crystals growing in areas of variable geochemical conditions. Evidence for crystal fractionation in episode III has been postulated and, therefore, may result in the release of latent heat and subsequent melting of surrounding wallrock. Therefore, magmatic convection results in the migration of crystal populations to areas of lower anorthite content, potentially near the periphery of the magma chamber. Higher anorthitic regions of the crystals could be migration into less contaminated regions.

Microlites have lower anorthite contents compared to microphenocrysts and phenocrysts (Figure 31). Microlites likely reflect the chemical make-up of melt during

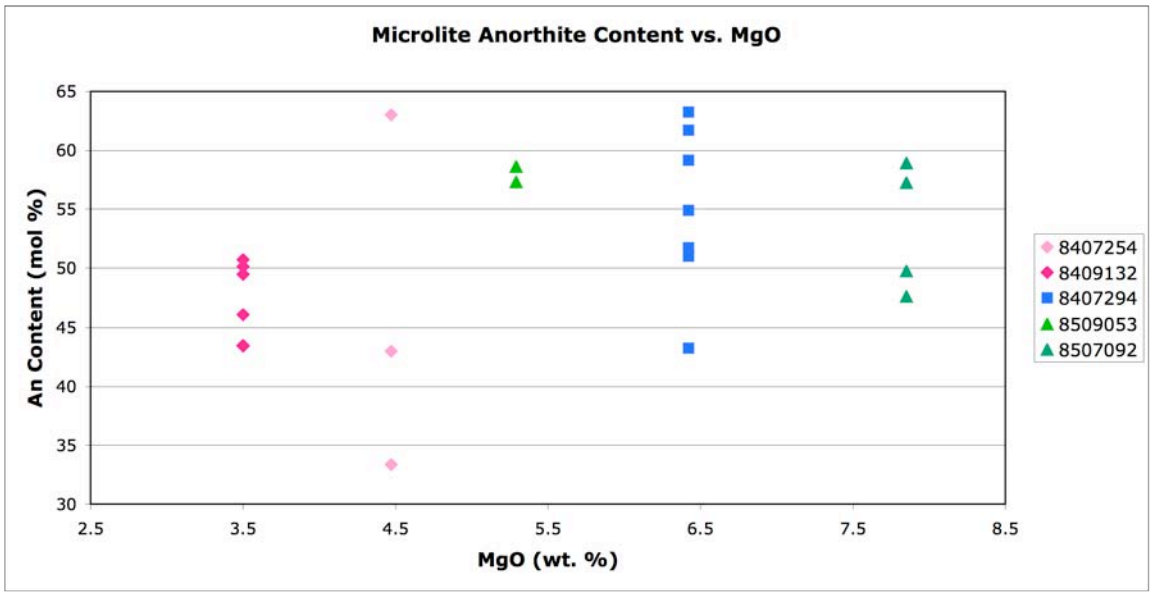

Figure 31. Binary plot of microlite anorthite content versus MgO.

ascent and are thus the last type of crystal to form. Average microlite anorthite content ranges from An_{46} to An_{58} mol %. It is shown in Figure 31 that the microlites of sample 8407254 have the largest range in anorthite content, from An_{33} to An_{63}.

Single Crystal Sr Isotope Ratios

Crystals from two samples, Bachelor Cap and Kwohl Butte, were analyzed for Sr isotope ratios. Analyses from sample 8409132 (Bachelor Cap), shown in Figure 24, are typically homogeneous with the whole-rock $^{87}Sr/^{86}Sr$ value and only three crystals that have higher values than the rest. Samples from 8507092 (Kwohl Butte) are typically homogenous with each other, but have lower values than the whole-rock $^{87}Sr/^{86}Sr$ value. One plagioclase crystal and both samples of the unidentified white material are not in equilibrium with the whole-rock values.

Single crystals from sample 8409132 (Bachelor Cap) included plagioclase feldspar and olivine. As seen in Figure 24, the olivine crystals and most of the plagioclase crystals were homogenous with the whole-rock $^{87}Sr/^{86}Sr$ isotope value. However, three crystals have significantly higher $^{87}Sr/^{86}Sr$ isotope ratios than the remaining crystals and whole-rock. The higher isotope ratio could be a result of magmatic convection during crystal growth (Singer et al., 1995). These crystals may have formed near the periphery of the magma chamber, where they were more impacted by assimilation. Once these crystals were formed, or partially formed, they migrated closer to a crystal population that had not experienced as much assimilation.

The analyses from sample 8507092 (Kwohl Butte) are typically not in equilibrium with the whole-rock value. Most of the plagioclase crystals are in equilibrium with each other, but have a lower Sr isotope value than the whole-rock. One plagioclase feldspar crystal is higher than the whole-rock value. The isotopic disequilibrium shown in Figure 25 could be a result of open-system processes affecting the older Kwohl Butte magmas. Because the isotope values for the individual crystals are typically lower than the whole-rock value, it can be proposed that assimilation may have occurred late in crystal formation or after the formation these crystals. The plagioclase crystal with a higher value could be a xenocryst of incorporated crustal material, as there does not seem to be significant evidence for magma recharge.

Two samples of unidentified white material are also not in equilibrium with the whole-rock value. One sample is significantly higher than the whole-rock value (0.704890 ± 33), whereas the other sample is lower than the whole-rock value (0.703418

± 8). The samples were completely destroyed during the digestion process, therefore no further analyses can be made on the substance to determine its composition. This material could have been plagioclase feldspar that has undergone weathering, resulting in the leaching and breakdown of the crystal structure. If this were the case, the expected $^{87}Sr/^{86}Sr$ value should be similar to that of the surrounding plagioclase crystals. This, however, does not seem to be the case. It could also be incorporated crustal material that was not completely melted prior to the lava cooling. If this hypothesis were true, expected isotopic ratios would be dissimilar from the whole-rock or surrounding plagioclase crystals. This latter hypothesis seems to comply with the data obtained from these samples of white material. It can be hypothesized that before or upon eruption, surrounding crustal material was incorporated into the erupting lava at least during activity at Kwohl Butte. The impact this type of material may have on the whole-rock isotope value is a factor that must be considered when assessing the role of isotope ratio variation in the lavas.

The $^{87}Sr/^{86}Sr$ values obtained for the single crystals suggest that open-system processes, most likely from crustal contamination, significantly affected the magmas of Kwohl Butte. There is evidence of possible assimilation occurring during the formation of lavas from the Bachelor Cap, although most samples are in isotopic equilibrium with the whole-rock value. The evidence provided by single crystal isotope analysis concurs with the proposed suggestion of physically separated magma chambers for the Kwohl Butte and Bachelor Cap lavas.

Magmatic Processes During Episode III

By analyzing both whole-rock and single crystal components of this suite of lavas, hypotheses about the system in which these lavas formed can be assessed. It is apparent from the whole-rock data that crystal fractionation has a significant influence on the lavas erupted. However, there is evidence of the influences of open-system processes through whole-rock isotopic data, both in $^{87}Sr/^{86}Sr$ and $^{143}Nd/^{144}Nd$. When compared to single crystal isotopes, it is apparent that generally, little open-system processes have affected the individual grains within both the older Kwohl Butte and the younger Bachelor Cap. The minor isotopic variations are attributed to magmatic convection and AFC processes.

Geochemical data obtained from major and trace elements indicate the evolution of the lavas through the crystal fractionation of clinopyroxene, olivine, Fe–Ti oxides, and apatite. Plagioclase feldspar was stable, but did not efficiently separate. However, there is an obvious distinction between the older and younger units with respect to these data. The younger lavas all show more evolved chemistries, alluding to the higher degree of differentiation during the formation of these magmas.

Single crystal geochemistry obtained through electron microprobe demonstrates the relatively simple system in which these crystals formed. This is also observed in the textures illustrated by NDIC imaging. There is evidence that areas of some of the crystals grew in more evolved conditions, potentially as a result of magmatic convection to locations along the periphery of the magma chamber where crustal contamination was occurring.

Evidence from whole-rock isotope values suggests that physically separated magma systems could have existed for the older Kwohl Butte and Bachelor Shield units and the younger Bachelor Cap and Tot Mountain units. This could be the result of several magma chambers evolving independently, thus resulting in isotopically and geochemically distinct lavas. Alternatively, the continued evolution evidenced by both isotopic ratios and geochemical analyses could indicate one evolving system. The shift from less evolved to more evolved lavas during episode III supports the hypothesis of one magma system. Computer modeling with programs such as MELTS (Ghiorso and Sack, 1995) could provide the necessary assessment of the chemical properties of the magma system. Regardless of the properties of the magmatic plumbing system, the active system during episode III existed in a generally closed system with only minor amounts of assimilation of crustal material and little evidence for recharge events.

Evidence for minor magma recharge is observed by isotopic analyses. Within individual lava units, specifically Kwohl Butte and Bachelor Shield, decreases in $^{87}Sr/^{86}Sr$ and increases in $^{143}Nd/^{144}Nd$ values can be observed between the relative ages, indicating the potential influence of minor recharge events. Similarly, a magma recharge event could account for the isotopic disequilibrium observed in the plagioclase feldspar crystals from Kwohl Butte. Until further studies are completed, it is still difficult to assess the extent to which magma recharge contributed to the isotopic disequilibrium observed in the older Kwohl and Bachelor Shield lavas.

The proposed petrogenetic model according to Gardner (1994b) indicated the possible presence of several magma chambers and conduits, allowing magma mixing to

occur on a spatial scale over the course of activity at the MBVC. It was speculated that the geochemical diversity observed throughout the MBVC was caused by continuous crystal fractionation and periodic magma replenishment, with minor amounts of assimilation of crustal material. Interpretations presented here for episode III shared some similarities with the Gardner model, specifically continuous crystal fractionation. There is evidence for open-system processes in the form of assimilation of surrounding country rock. Isotope values suggest that recharge may have affected early lavas. Based on data presented here, continuous recharge does not appear to be a critical process in the younger lavas. The data presented here provide evidence for a complex magma chamber system existing during activity at the MBVC throughout episode III.

Mafic Magmatism in the High Cascades Region

It has been discussed previously that the MBVC is situated in the central Oregon High Cascades, an area that experiences not only convergence of the Juan de Fuca and North American plate, but also extension by rifting that began around 7–8 Ma (Conrey et al., 1997). It has been proposed that this tectonic setting results in the mafic magmatism observed along the central Oregon High Cascades and specifically at the MBVC (Hughes and Taylor, 1986; Conrey et al., 1997). The results presented here provide more evidence for a complex magma system at the MBVC, as initially proposed by Gardner (1994b). Geochemical diversity exists in this region, resulting in variation in lava compositions within the central Oregon High Cascades. For instance, South Sister, a volcano 20 mi north of the MBVC, is composed of lavas ranging from basalt (50 wt % SiO_2) to rhyolite (75 wt % SiO_2) (Brophy and Dreher, 2000). Such extremely silicic lavas are not found at

the MBVC but have been attributed to continuous crystal fractionation and crustal melting and assimilation (Brophy and Dreher, 2000).

Because of the complex nature of volcanic activity, understanding of magmatic processes is imperative for hazard mitigation. The MBVC is situated in a highly complex tectonic setting and therefore warrants a need for better understanding of the triggers that result in volcanic activity. Although activity at the MBVC has subsided, there is potential for surrounding areas to reactivate. Assessment of magmatic processes, such as magmatic recharge or assimilation, as well as modeling of the magmatic plumbing system is imperative. The results from this study coupled with the work done by Gardner (1994b) have demonstrated that the magma system under the MBVC is shallow and may be composed of several independent magma chambers, some of which interact with each other, some of which are independent of each other. If activity were to reactivate, thus triggering continued activity in this region, potential hazards could threaten surrounding populations. It is for this reason continued research at this tectonically active region is significant.

CHAPTER VI

CONCLUSIONS

Overview

The objective of this study was to utilize several chemical properties from the lavas of episode III of the MBVC to further elucidate the magmatic processes that have influenced the evolution of the associated magmatic system. Studies at the MBVC by Gardner (1994b) suggested that the magma system was composed of several independent magma bodies in which minor magma recharge and crystal fractionation were the most prevalent processes. My study has contributed significant data, including much needed isotopic ratio data, to the existing datasets, as well as providing intriguing questions concerning the extent of magma evolution at the MBVC. Results from this study support the role of crystal fractionation, as well as the complexities of the magmatic system located under the MBVC initially presented by Gardner. Incorporation of whole-rock and single crystal data has provided a clearer picture of the role of open- versus closed-system magmatic processes associated with the MBVC.

Evidence for Assimilation

Potential assimilation processes are evidenced by radiogenic isotopic disequilibrium. This disequilibrium is observed in the Sr and Nd isotope analyses of whole-rock samples among the individual units and throughout the entire episode III sequence. A trend of isotopic evolution is observed with increased $^{87}Sr/^{86}Sr$ and decreased $^{143}Nd/^{144}Nd$ from the Kwohl Butte to the Tot Mountain lavas. The trend of

evolution is attributed to the latent heat released during crystal fractionation and the consequential assimilation of surrounding country rock into the magma.

Single crystal isotope ratios collected from the oldest and youngest lava units also provide evidence for the influence of assimilation. The older Kwohl Butte shows isotopic disequilibrium between the single crystals and the whole-rock isotope values. There is also evidence for the incorporation of potential crustal material in the erupted lava. The younger Bachelor Cap lava shows more isotopic equilibrium between the single crystals and whole-rock sample. The isotopic equilibrium that exists between the single crystals and whole-rock samples suggests that the magma system in which the crystals of Bachelor Cap grew did not experience as significant open-system processes as the magma of Kwohl Butte. There is also evidence for the possibility of independent systems in the radiogenic isotopes.

Evidence for Crystal Fractionation

Oxides and trace element data provide evidence for crystal fractionation of olivine and clinopyroxene as a significant process during the formation of the entire suite of rocks from episode III. These data do not support separation of plagioclase feldspar during magma evolution, although the possibility does exist that plagioclase was stable, but did not separate from the melt. Alternatively, the presence of plagioclase in the lavas could be attributed to accumulation during eruption. Petrographic analysis confirms the presence of accessory minerals, including Fe-Ti oxides and apatite. The fractionation of these minerals is further supported by the geochemistry.

NDIC images and petrographic analysis defined three gradations of crystal textures, defined by the level of complexity, including simple oscillatory zoning, intermediate and complex textures that include sieved textures and areas of resorption. Oscillatory zoning was observed in both microphenocrysts and phenocrysts, and is defined by 5–15 mol % change in An along a 10–20 μm distance. In terms of crystal classes, the range of An content for phenocrysts is An_{61} to An_{76}, for microphenocrysts is An_{55} to An_{75}, and for microlites is An_{37} to An_{55}. All crystal textures are found in all lava units.

Distinctions Between Kwohl Butte–Bachelor Shield and Bachelor Cap–Tot Mountain

The conclusions of this work are that all units of episode III experienced geochemical diversity as a result of crystal fractionation in a dominantly closed-magmatic system. Assimilation occurred with the release of latent heat associated with the process of crystal fractionation. The exchange of this heat with the surrounding country rock caused the incorporation of some contaminant melt into the system. The presence of plagioclase feldspar in the lavas of episode III is likely a result of inefficient separation. Geochemical and radiogenic isotopic distinctions exist between the Kwohl Butte–Bachelor Shield and Bachelor Cap–Tot Mountain units, suggesting that the associated magma chambers may be physically distinct. I hypothesize that the magma plumbing system at the MBVC during episode III was complex, involving at least two distinct systems, both of which were experiencing intense crystal fractionation.

Future Work

The data provided by this study yield a strong base for continued study of the MBVC. More analyses of the lavas of episode III, including more single crystal and *in situ* isotope analyses will provide detailed understanding of the magma system. Geochemical computer modeling, such as MELTS and EC–RAFC (Ghiorso and Sack, 1995; Bohrson and Spera, 2001; Bohrson et al., 2005,), have been used to understand the degree of assimilation from major and trace element and isotope data and could greatly contribute to the understanding of the magmatic systems located at the MBVC. Further studies on the remaining three episodes could provide a more complete understanding of the MBVC, and should, therefore, be the next priority for work at this location. In depth studies of the remaining three episodes would provide significantly more information regarding this complex volcanic system and perhaps shed more light on the relationship among magma systems in the Oregon High Cascades region.

REFERENCES CITED

Anderson, A.T., 1983, Oscillatory zoning of plagioclase: Nomarski interference contrast microscopy of etched polished sections: American Mineralogist, v. 68, p. 125–129.

Bacon, C.R., 1983, Eruptive history of Mount Mazama and Crater Lake caldera, Cascade Range, U.S.A.: Journal of Volcanology and Geothermal Research, v. 18, p. 57–115.

Bacon, C.R., 1990, Calc-alkaline, shoshonitic, and primitive tholeiitic lavas from monogenetic volcanoes near Crater Lake, Oregon: Journal of Petrology, v. 31, p. 135–166.

Bacon, C.R, Bruggman, P.E., Christiansen, R.L., Clynne, M.A., Donnelly-Nolan, J.M., and Hildreth, W., 1997, Primitive magmas at five Cascade volcanic fields: Melts from hot, heterogeneous sub-arc mantle: The Canadian Mineralogist, v. 35, p. 397–423.

Bohrson, W.A., and Spera, F.J., 2001, Energy-constrained open-system magmatic processes II: Application of energy-constrained assimilation-fractional crystallization (EC-AFC) model to magmatic systems: Journal of Petrology, v. 42, n. 5, p. 1019–1041.

Bohrson, W.A., and Spera, F.J., 2003, Energy-constrained open-system magmatic processes IV: Geochemical thermal and mass consequences of energy-constrained recharge, assimilation and fractional crystallization (EC-RAFC): Geochemistry Geophysics, Geosystems, v. 4, n. 2, 10.1029/2002GC000316.

Bowen, N.L., 1928, The evolution of the igneous rocks, Princeton, NJ: Princeton University Press, 334 p.

Brophy, J.G., and Dreher, S.T., 2000, The origin of composition gaps at South Sister volcano, central Oregon: Implications for fractional crystallization processes beneath active calc-alkaline volcanoes: Journal of Volcanology and Geothermal Research, v. 102, p. 287–307.

Champion, D.E., 1980, Holocene geomagnetic secular variation in the western United States: Implications for the global geomagnetic field: U.S. Geological Survey Open-File Report-80–824, 277 p.

Conrey, R.M., Sherrod, D.R., Hooper, P.R., and Swanson, D.A., 1997, Diverse primitive magmas in the Cascade arc, northern Oregon and southern Washington: The Canadian Mineralogist, v. 35, p. 367–396.

Crock, J.G., and Lichte, F.E., 1982, Determination of rare earth elements in geological materials in inductively coupled argon plasma/atomic emission spectrometry: Analytical Chemistry, v. 54, p. 1329–1332.

Davidson, J.P., Hora, J.M., Garrison, J.M., and Dungan, M.A., 2005, Crustal forensics in arc magmas: Journal of Volcanology and Geothermal Research, v. 140, p. 157–170.

Faure, G., and Mensing, T.M., 2004, Isotopes: Principles and applications, 3rd ed.: Hoboken, John Wiley and Sons, Inc., 347 p.

Fleck, R.J., 1990, Neodymium, strontium, and trace element evidence of crustal anatexis and magma mixing in the Idaho batholith, *in* Anderson, J.L., ed., The nature and origin of Cordilleran magmatism (Memoir 174): Boulder, Colorado, Geological Society of America.

Fowler, S.J, Bohrson, W.A., and Spera, F.J., 2004, Magmatic evolution of the Skye Igneous Centre, Western Scotland: Modeling of assimilation, recharge, and fractional crystallization: Journal of Petrology, v. 45, n. 12, p. 2481–2505.

Gardner, C.A., 1994a, Paleomagnetic and petrologic sample location map for the Mount Bachelor Volcanic Chain, Cascades Range, Oregon: U.S. Geological Survey Miscellaneous Investigations, scale 1:24,000.

Gardner, C.A., 1994b, Temporal, spatial and petrologic variations of lava flows from the Mount Bachelor volcanic chain, central Oregon High Cascades: USGS Open File Report, v. 94–261, 100 p.

Ghiorso, M.S., and Sack, R.O., 1995, Chemical mass transfer in magmatic processes IV. A revised and internally consistent thermodynamic model for the interpolation and extrapolation of liquid-solid equilibria in magmatic systems at elevated temperatures and pressures: Contributions to Mineralogy and Petrology, v. 119, n. 2–3, p. 197–212.

Ginibre, C., Woerner, G., and Kronz, A., 2007, Crystal zoning as an archive for magma evolution: Elements, v. 3, p. 261–266.

Green, N.L., and Sinha, A.K., 2005, Consequences of varied slab age and thermal structure on enrichment processes in the sub-arc mantle of the northern Cascadia subduction system: Journal of Volcanology and Geothermal Research, v. 140, p. 107–132.

Haase, C.S., Chadam, J., Feinn, D., and Ortoleva, P., 1980, Oscillatory zoning in plagioclase feldspar: Science, v. 209, p. 272–274.

Hughes, S.S., and Taylor, E.M., 1986, Geochemistry, petrogenesis, and tectonic implications of central High Cascade mafic platform lavas: Geological Society of America Bulletin, v. 97, p. 1024–1036.

Knaack, C., Cornelius, S.B., and Hooper, P.R., 1994, Trace element analyses of rocks and minerals by ICP-MS: GeoAnalytical Lab, Washington State University.

Kohut, E.J. and Nielson, R.L., 2003, Low-pressure phase equilibria of anhydrous anorthite-bearing mafic magmas: Geochemistry, Geophysics, Geosystems, v. 4, 10.1029/2002GC000451.

Leeman, W.P., Lewis, J.F., Evarts, R.C., Conrey, R.M., and Streck, M.J., 2005, Petrologic constraints on the thermal structure of the Cascades arc: Journal of Volcanology and Geothermal Research, v. 140, p. 67–105.

Lichte, F.E., Meier, A.L., and Crock, J.G., 1987, Determination of the rare-earth elements in geological materials by inductively coupled plasma mass spectrometry: Analytical Chemistry, v. 59, p. 1150–1157.

Lundstrom, C.C., and Tepley, F.J., 2006, Investigating the origin of anorthitic plagioclase through a combination of experiments and natural observations: Journal of Volcanology and Geothermal Research, v. 157, p. 202–221.

Moore, A.C., 1969, A method for determining mineral compositions by measurement of the mass absorption coefficient: American Mineralogist, v. 43, p. 1180–1189.

Pearce, T.H. and Kolisnik, A.M., 1990, Observations of plagioclase zoning using interference imaging: Earth-Science Reviews, v. 29, p. 9–26.

Ramos, F.C., and Conrey, R.M., 2006, unpublished data.

Ramos, F.C., and Reid, M.R., 2005, Distinguishing melting of heterogeneous mantle sources from crustal contamination: Insights from Sr Isotopes at the phenocryst scale, Pisgah Crater, California: Journal of Petrology, v. 46, n. 5, p. 999–1012.

Ramos, F.C., Wolff, J.A., and Tollstrup, D.L., 2005, Sr isotope disequilibrium in Columbia River flood basalts: Evidence for rapid shallow-level open-system processes: Geology, v. 33, n. 6, p. 457–460.

Rollinson, H., 1993, Using geochemical data: Evaluation, presentation, interpretation: Essex, England, Longman Scientific and Technical, 108 p.

Schmidt, M.E., Grunder, A.L., and Rowe, M.C., 2008, Segmentation of the Cascade arc as indicated by Sr and Nd isotopic variation among diverse primitive basalts: Earth and Planetary Science Letters, v. 266, p. 166–181.

Scott, W.E., 1990, Temporal relations between eruptions of the Mount Bachelor volcanic chain and fluctuations of late Quaternary glaciers: Oregon Geology, v. 52, n. 5, p. 114–117.

Scott, W.E., and Gardner, C.A., 1990, Field trip guide to the central Oregon High Cascades, Part 1: Mount Bachelor-South Sister area: Oregon Geology, v. 52, n. 5, p. 99–114.

Scott, W.E., and Gardner, C.A., 1992, Geologic map of the Mount Bachelor volcanic chain and surrounding area, Cascade Range, Oregon: U.S. Geological Survey Miscellaneous Investigations Map I–196, scale 1:50,000.

Scott, W.E., Gardner, C.A., and Sarna-Wojcicki, A.M., eds., 1989, Guidebook for field trip to the mount Bachelor-South Sister-Bend area, central Oregon High Cascades: U.S. Geological Survey Open-File Report 89–645, 66 p.

Singer, B.S., Dungan, M.A., and Layne, G.D., 1995, Textures and Sr, Ba, Mg, Fe, K, and Ti compositional profiles in volcanic plagioclase: Clues to the dynamics of calc-alkaline magma chambers: American Mineralogist, v. 80, p. 776–798.

Spera, F.J., and Bohrson, W.A., 2001, Energy-constrained open-system magmatic processes I: General model and energy-constrained assimilation and fractional crystallization (EC-AFC) formulation: Journal of Petrology, v. 42, n. 5, p. 999–1018.

Spera, F.J., and Bohrson, W.A., 2002, Energy-constrained open-system magmatic processes 3. Energy-constrained recharge, assimilation, and fractional crystallization (EC-RAFC): Geochemistry Geophysics, Geosystems, v. 3, n. 12, 10.1029/2002GC000315.

Sun, S.S., and McDonough, W.F., 1989, Chemical and isotopic systematics of oceanic basalts: implications for mantle composition and processes, *in* Saunders, A.D., and Norry, M.J., eds., Magmatism in the ocean basins: Geological Society Special Publication, n. 42, p. 313–345.

Tanton, L.T.E., Grove, T.L., and Donnelly-Nolan, J., 2001, Hot, shallow mantle melting under the Cascades volcanic arc: Geology, v. 29, n. 7, p. 631–634.

Tepley, F.J., Davidson, J.P., and Clynne, M.A., 1999, Magmatic interactions as recorded in plagioclase phenocrysts of Chaos Crags, Lassen Volcanic Center, California: Journal of Petrology, v. 40, n. 5, p. 787–806.

Topinka, L., 1997, Central Oregon High Cascades: USGS/CVO: http://vulcan.wr.usgs .gov/Volcanoes/Oregon/HighCascades/Maps/map_high_cascades.html, 8 April 2008.

Turner, S., George, R., Jerram, D.A., Carpenter, N., and Hawkesworth, C., 2003, Case studies of plagioclase growth and residence times in island arc lavas from Tonga and the Lesser Antilles, and a model to reconcile discordant age information: Earth and Planetary Science Letters, v. 214, p. 279–294.

Wilson, B.M., 1989, Igneous petrogensis: A global tectonic approach: Dordrecht, Netherlands, Springer, p. 17–21.

Winter, J.D., 2001, An introduction to igneous and metamorphic petrology: Upper Saddle River, Prentice Hall, p. 160–164.

Zellmar, G.F., Annen, C., Charlier, B.L.A., George, R.M.M., Turner, S.P., and Hawkesworth, C.J., 2005, Magma evolution and ascent at volcanic arcs: Constraining petrogenetic processes through rates and chronologies: Journal of Volcanology and Geothermal Research, v. 140, p. 171–191.